

Pivotal role of PIM2 kinase in plasmablast generation and plasma cell survival, opening new treatment options in myeloma

Marion Haas, Gersende Caron, Fabrice Chatonnet, Stephane Manenti, Elina Alaterre, Julie Devin, Céline Delaloy, Giulia Bertolin, Roselyne Viel, Amandine Pignarre, et al.

▶ **To cite this version:**

Marion Haas, Gersende Caron, Fabrice Chatonnet, Stephane Manenti, Elina Alaterre, et al.. Pivotal role of PIM2 kinase in plasmablast generation and plasma cell survival, opening new treatment options in myeloma. Blood, 2022, 139 (15), pp.2316-2337. 10.1182/blood.2021014011 . hal-03578490

HAL Id: hal-03578490
https://hal.science/hal-03578490

Submitted on 1 Apr 2022

HAL is a multi-disciplinary open access archive for the deposit and dissemination of scientific research documents, whether they are published or not. The documents may come from teaching and research institutions in France or abroad, or from public or private research centers.

L'archive ouverte pluridisciplinaire **HAL**, est destinée au dépôt et à la diffusion de documents scientifiques de niveau recherche, publiés ou non, émanant des établissements d'enseignement et de recherche français ou étrangers, des laboratoires publics ou privés.



Distributed under a Creative Commons Attribution - NonCommercial 4.0 International License

Pivotal role of PIM2 kinase in plasmablast generation and plasma cell survival, opening new treatment options in myeloma

Tracking no: BLD-2021-014011R2

Marion Haas (INSERM_U1236, university Rennes 1, EFS Bretagne and university hospital, France) Gersende Caron (INSERM U917, France) Fabrice Chatonnet (Centre Hospitalier Universitaire de Rennes, France) stephane manenti (INSERM U1037, France) Elina Alaterre (Institute of Human Genetics, France) Julie Devin (Université de Toulouse, France) Céline Delaloy (INSERM_U1236, university Rennes 1, France) Giulia Bertolin (Université de Rennes, CNRS, Institut de Génétique et Développement de Rennes (IGDR), UMR 6290, France) Roselyne Viel (Université Rennes 1, H2P2, France) Amandine Pignarre (INSERM_U1236, university Rennes 1, EFS Bretagne and university hospital, France) Francisco Llamas Gutierrez (university hopistal of Rennes, France) Anne Marchalot (Université de Limoges, UMR CNRS 7276, INSERM U1262, France) Olivier Decaux (CHU de Rennes, France) Karin Tarte (Faculté de Médecine, France) Laurent Delpy (CNRS, France) Jerome Moreaux (Institute of Human Genetics, France) Thierry Fest (INSERM_U1236, university Rennes 1, EFS Bretagne and university hospital, France)

Abstract:
The differentiation of B cells into plasmablasts (PBs) and then plasma cells (PCs) is associated with extensive cell reprogramming and new cell functions. By using specific inhibition strategies (including a novel morpholino RNA antisense approach), we found that early, sustained upregulation of the proviral integrations of Moloney virus 2 (PIM2) kinase is a pivotal event during human B cell *in vitro* differentiation and then continues in mature normal and malignant PCs in the bone marrow. In particular, PIM2 sustained the G1/S transition by acting on CDC25A and $p27^{Kip1}$ and hindering caspase 3-driven apoptosis through BAD phosphorylation and cytoplasmic stabilization of $p21^{Cip1}$. In PCs, interleukin-6 triggered PIM2 expression, resulting in anti-apoptotic effects on which malignant PCs were particularly dependent. In multiple myeloma, pan-PIM and MCL1 inhibitors displayed synergistic activity. Our results highlight a cell-autonomous function that links kinase activity to the PBs' newly acquired secretion ability and the adaptability observed in both normal and malignant PCs, and finally should prompt the reconsideration of PIM2 as a therapeutic target in multiple myeloma.

Conflict of interest: COI declared - see note

COI notes: M.H., G.C., A.M., L.D., J.M. and T.F. have applied for a European patent on the use of an SSO to modulate PIM2 expression. The other authors have no conflicts of interest to declare.

Preprint server: No;

Author contributions and disclosures: M.H. designed and conducted the experiments, and wrote the paper; G.C. designed the cell differentiation model, and performed cytometry and cell-sorting; F.C. performed genomic analysis; E.A performed ChIP-qPCR STAT3 experiments; J.D. performed drug combination experiments; A.P. performed single-cell qPCRs; C.D. helped with BACH2 assays and discussed results; S.M. performed CDC25A immunoblotting; G.B. performed FRET experiments; R.V. performed immunostaining; F.L-G. provided bone marrow biopsies; A.M. designed morpholino SSO; O.D. provided multiple myeloma samples; K.T. discussed results; L.D. provided the antisense strategy; J.M. provided cell lines and original data; T.F. designed and supervised the experiments, and wrote the paper.

Non-author contributions and disclosures: No;

Agreement to Share Publication-Related Data and Data Sharing Statement: GEO accession number GSE136990

ACCEPTED MANUSCRIPT - CLEAN COPY

Clinical trial registration information (if any):

ACCEPTED MANUSCRIPT - CLEAN COPY

***Title*:** Pivotal role of PIM2 kinase in plasmablast generation and plasma cell survival, opening new treatment options in myeloma

Authors: Marion Haas[1,2], Gersende Caron[1,2], Fabrice Chatonnet[1,2], Stéphane Manenti[3], Elina Alaterre[4], Julie Devin[3], Céline Delaloy[1], Giulia Bertolin[5], Roselyne Viel[6], Amandine Pignarre[1,2], Francisco Llamas-Gutierrez[7], Anne Marchalot[8], Olivier Decaux[1,9], Karin Tarte[1,2], Laurent Delpy[8], Jérôme Moreaux[4], and Thierry Fest[1,2,10]

Affiliations: [1] Université de Rennes 1, INSERM, Établissement Français du Sang de Bretagne, UMR_S1236, F-35043 Rennes, France; [2] Laboratoire d'hématologie et immunologie, Pôle de Biologie, Centre Hospitalier Universitaire, F-35033 Rennes, France; [3] Université de Toulouse, CNRS ERL 5294, INSERM U1037, Centre de Lutte Contre le Cancer (CRCT), F-31000 Toulouse, France; [4] Institut de Génétique Humaine, UMR 9002 CNRS-UM ; Pôle de biologie, Centre Hospitalier Universitaire, F-34000 Montpellier; [4] Université de Toulouse, CNRS ERL 5294, INSERM U1037, Centre de Lutte Contre le Cancer (CRCT), F-31000 Toulouse, France; [5] Université de Rennes, CNRS, Institut de Génétique & Développement de Rennes (IGDR) Rennes, UMR 6290, F-35000 France; [6] H2P2 Rennes, France; [7] Laboratoire d'Anatomie Pathologique, Pôle de Biologie, Centre Hospitalier Universitaire, F-35033 Rennes, France; [8] Université de Limoges, UMR CNRS 7276, INSERM U1262, F-87025 Limoges, France; [9] Service d'hématologie clinique, Centre Hospitalier Universitaire, F-35033 Rennes, France; [10] lead contact.

Correspondence: Thierry Fest, MD, PhD; INSERM U1236, Faculté de Médecine, 2 avenue du Pr Léon Bernard, CS 34317, 35043 Rennes Cedex, France
Phone: +33-299-284-127
Fax: + 33-299-284-152
E-mail : thierry.fest@univ-rennes1.fr
ORCID: https://orcid.org/0000-0002-6437-4189

Running title: PIM2 kinase and plasma cells

Primary research article

Word count (Introduction, Methods, Results and Discussion): 4164

Figure count: 7

Reference count: 52

The manuscript includes Supplemental Information and Supplemental Figures.

Key points

- B cell commitment into plasmablasts activates *PIM2* via STAT3, which promotes G1/S transition and inhibits caspase 3-driven apoptosis.
- Plasma cell survival requires strong expression of PIM2 & its inhibition exhibits a synergistic effect with MCL1 inhibitor in myeloma.

SUMMARY

The differentiation of B cells into plasmablasts (PBs) and then plasma cells (PCs) is associated with extensive cell reprogramming and new cell functions. By using specific inhibition strategies (including a novel morpholino RNA antisense approach), we found that early, sustained upregulation of the proviral integrations of Moloney virus 2 (PIM2) kinase is a pivotal event during human B cell *in vitro* differentiation and then continues in mature normal and malignant PCs in the bone marrow. In particular, PIM2 sustained the G1/S transition by acting on CDC25A and $p27^{Kip1}$ and hindering caspase 3-driven apoptosis through BAD phosphorylation and cytoplasmic stabilization of $p21^{Cip1}$. In PCs, interleukin-6 triggered PIM2 expression, resulting in anti-apoptotic effects on which malignant PCs were particularly dependent. In multiple myeloma, pan-PIM and MCL1 inhibitors displayed synergistic activity. Our results highlight a cell-autonomous function that links kinase activity to the PBs' newly acquired secretion ability and the adaptability observed in both normal and malignant PCs, and finally should prompt the reconsideration of PIM2 as a therapeutic target in multiple myeloma.

Keywords: PIM2 kinase, B cell differentiation, plasma cell, G1/S transition, apoptosis, caspase 3, MCL1, multiple myeloma

INTRODUCTION

Before becoming plasma cells (PCs), the B cells first pass through an immature, proliferative plasmablast (PB) stage. The PBs emerge after major changes in the B cells' morphology, epigenome-sustained expression profile, and lifespan[1,2]. This tightly regulated cell metamorphosis can be hijacked by oncogenic alterations that drive malignant transformation. Although there is a large body of data on normal B cell differentiation, studies of B cell malignancies have shown that our understanding of normal B cell function is incomplete[3] in particular for identifying specific factors and determining their spatiotemporal involvement in the molecular modifications underlying B cell metamorphosis.

We recently reported that the emergence of human PBs is associated with large-scale methylome modifications, with the local acquisition of active epigenetic marks on PC identity genes during a committal step in which some activated B cells differentiate into PBs[4]. These highly proliferative, activated, committed B cells (hereafter referred to as preplasmablasts (prePBs)) are characterized by the silencing of the IL-4/STAT6 pathway and thus downregulation of CD23 surface marker expression[5]. By focusing on this feature, a comparative RNA sequencing (RNA-seq) analysis of prePBs allowed us to identify here a striking increase in expression of the gene encoding the proviral integrations of Moloney virus 2 (PIM2) serine/threonine kinase. The three member of the PIM kinase family are known to phosphorylate numerous substrates involved in crucial cellular functions[6]. Dysregulated expression of PIM kinases has been reported in several cancers including multiple myeloma (MM)[7,8]. Surprisingly, PIM2 has never been analyzed in the context of normal B cell differentiation. In mouse pro-B cells,

Pim2 expression depends of growth-factor-induced transcription[9,10], which justifies further research in the context of PC differentiation.

In the present study, we evaluated the effects of PIM2 on PB generation and PC survival. We found that the B cell commitment activates the transcription of *PIM2* in a STAT3-dependent manner, which leads to a strong increase in the protein's expression level and functional activity. We assessed PIM2's biological effects in primary B cells by comparing a normal culture with two conditions in which PIM2's functions were altered by either stopping gene expression or blocking kinase activity. Along with PIM2-mediated BAD phosphorylation, we detected effects on $p21^{Cip1}$, CDC25A and $p27^{Kip1}$. During the final step in differentiation, these effects all promote cell survival and entry into the S-phase of the cell cycle. Moreover, PIM2 was found strongly expressed in quiescent mature PCs and essential for cell survival. In malignant setting, PCs are addicted to PIM2 and targeting this kinase was synergistic with BH3-mimetic offering new treatment options for MM.

METHODS

Purification of primary B cells, cell culture, cell cycle assessment, immunophenotyping, cell sorting and protein assays. Procedures and methods were detailed in Supplemental Methods.

Cell lines culture and viability assays. Human myeloma cell lines were obtained and cultured as described in[11]. Viability was assessed for cells treated with selected compounds: AZD1208 & AZD5991 (Selleckchem). CellTiter-Glo® Luminescent Assay kit (Promega) was used as described by the manufacturer. Results were normalized to the samples without treatment and synergy score were calculated using the Bliss method[12] as described in[13].

Primary MM cells. Samples have been collected with the approval of the institutional research board from Rennes university hospital and in accordance with the Declaration of Helsinki. Mononuclear cells were isolated using Ficoll density gradient centrifugation. Samples were cultured in presence of 2 ng/mL IL-6. Cell cytotoxicity was evaluated by flow cytometry by determining the percentage of viable $CD138^+$ cells.

SSO experiments. Inhibition of PIM2 expression is enabled by the use of a vivo-morpholino PIM2 splice-switching antisense oligonucleotide (SSO-PIM2) from Gene Tools, LLC (Philomath, OR, US). An irrelevant vivo-morpholino standard oligonucleotide was used as control (SSO-CTL). PIM2 mRNA knockdown efficiency was evaluated by RT-PCR to simultaneously identify full length (286 pb) and alternatively spliced (176 bp) PIM2 mRNAs on an agarose gel. Quantification of inhibition was also performed by RT-qPCR with exon 2 targeting primers and verified at the protein level by immunoblot.

RNA-Sequencing, ATAC-sequencing and data accessibility. Procedures and analysis methods were described in[5]. Raw data are accessible under GEO accession number GSE136990.

RESULTS

The emergence of PIM2 expression during plasmablast commitment

To identify genes regulated specifically during the final commitment step, we used our previously described *in vitro* differentiation model with human naive B cells (NBCs) generating four cell populations on day (D) 6 (Fig. 1A)[14]. The RNA-seq data (confirmed by qPCR assays) revealed a striking elevation of *PIM2* mRNA expression (but not *PIM1* or *PIM3* expression) in prePBs (P2/CD23$^-$ population) and PBs (P1 population), relative to B cells diverted from differentiation (P2/CD23$^+$ and P3 populations) (Fig. 1B and Fig. S1A). In an unsupervised analysis, the results of single-cell RT-qPCRs in P2/CD23$^-$ vs. P2/CD23$^+$ cell populations ranked *PIM2* as the most discriminating gene – ahead of *PRDM1* (Fig. 1C and Fig. S1B). Analysis of our RNA-seq datasets showed that *PIM2* was in the top 150 genes characterizing PBs, relative to noncommitted B cell populations (Fig. S1C)[5]. The protein levels correlated perfectly with gene expression levels, with strong PIM2 expression in prePBs and PBs (Fig. 1B). With regard to human tonsil-derived cell populations, CD19$^+$IgD$^-$CD38^{bright} PBs expressed higher levels of PIM2 than other B cell populations (Fig. 1D).

To determine whether *PIM2* gene expression is coupled to genomic changes during PC differentiation, we analyzed our previously published datasets[4,5] and ENCODE annotations (https://www.encodeproject.org). An assay for transposase-accessible chromatin using sequencing (ATAC-seq) showed that the open regions in prePBs and PBs included the *PIM2* promoter and an upstream enhancer. This latter overlaps with a region denoted as interacting physically with the *PIM2* promoter in the FANTOM5 database[15] and with a super-enhancer described in PBs and MM PCs (Fig. 1E)[16]. The comparative analysis of genome-wide 5hmC marks in NBCs vs. PBs showed that read

densities increased in both the identified ATAC-seq regions and the body of the *PIM2* sequence; this testified to the enhancer functions and activation in PBs, as has been shown for PB/PC identity genes (Fig. 1E and Fig. S1D)[4].

ATAC-seq analysis showed that the time course of promoter opening did not match the gene expression pattern; this disparity suggests that a transcriptional regulator is present in the *PIM2* locus (Fig. 1E and Fig. S1D). By chromatin immunoprecipitation (ChIP) sequencing human activated B cells, we identified a BACH2 binding site in the *PIM2* promoter[17]. BACH2 inhibition experiments showed a subsequent increase in PIM2 expression and thus confirmed that BACH2 acts as a repressor (Fig. 1F). Furthermore, the stimulation of PBs with IL-10, IL-21 and (to a lesser extent) IL-6 resulted in a sharp induction of PIM2 expression (Fig. 1G). Given that all three cytokines are known to recruit the STAT3 pathway, we exposed the cells to the STAT3 inhibitor C188-9; this led to the dose-dependent repression of PIM2 expression (Fig. 1G, H). In contrast, IL-2 (which recruits STAT5) and interferon-α were weak inducers (Fig. 1G). Since STAT3 signaling also induces *PRDM1*/BLIMP1 expression[18], we wondered if PIM2 was one of the downstream factors of BLIMP1. In fact, under IL-10 (or IL-21, data not shown) stimulation, *PRDM1* was induced but later than *PIM2* expression (Fig. S1E). In addition, siPRDM1 experiments on primary B cells and U266 MM cells showed no modifications in *PIM2* expression unlike the well-known target genes of BLIMP1 (Fig S1F-G)[19,20], consistent with previous data in prePB/PBs from knockout *Prdm1* mice[21]. Finally, by ChIP-qPCR on PBs and in RPMI8226 MM cells as well, we confirmed the binding of pSTAT3 on the *PIM2* promoter, as well on the intron 3 of *PIM2* locus (predicted enhancer region) and in the putative enhancer located downstream the gene (Fig. 1E and Fig. S1H). Altogether, these results confirmed that PIM2 respond directly to STAT3 and not via BLIMP1. Interestingly,

while PIM2-positive PBs were pSTAT3-positive in absence of BACH2, PIM2-negative/BACH2-positive CD23+ aBCs were also positive for pSTAT3 suggesting that the downregulation of BACH2 is required before STAT3 can induce PIM2 expression (Fig S1I).

Taken as a whole, our results demonstrate that PB differentiation is associated with a sharp elevation of PIM2 kinase expression; this elevation requires the removal of BACH2 repression and STAT3 activation (Fig. 1J).

PIM2 is required for the differentiation of B cells into PBs

To determine the functional involvement of PIM2 in the committal step and obtain further differentiated cells on D6, we focused our study on resulting PBs and $CD23^+$ post-activated B cells (hereafter referred to as $CD23^+$ aBCs), which both differed markedly in their PIM2 expression (Fig. 2A). In subsequent experiments, we compared a normal culture setting with conditions in which PIM2 was inhibited on D4 by exposure to the small-molecule pan-PIM inhibitor AZD1208 (hereafter referred as PIMi) or by specifically blocking *PIM2* gene expression using a novel antisense RNA strategy based on a morpholino splice-switching oligonucleotide (SSO) (Fig. 2B). Cells cultured with SSO-PIM2 exhibited a dose-dependent decrease in full-length *PIM2* mRNA - the expression of a weaker band corresponding to alternatively-spliced mRNAs lacking exon 2 – as well as PIM2 protein expression (Fig. 2C). At the selected dose of 2 µM, PIM2 expression was almost completely abrogated in PBs – without affecting *PIM1* expression (Fig. 2D and Fig S2B). While exposure to SSO-PIM2 did not affect the expression of key transcription factors involved in B cell differentiation (Fig. S2C), PIM2 knockdown led to a sharp decrease in PB generation (Fig. 2E,F and Fig. S2D). In

contrast, CD23^{+} aBCs were not affected. These results suggest that PIM2-kinase activity sustains the PB commitment.

PIM2 sustains the G1/S transition through an effect on CDC25A and p27^{Kip1}

A comparison of gene expression in prePBs vs. noncommitted B cell populations evidenced the downregulation of *SMAD3* in the former population. Accordingly, prePBs upregulated *CDC25A*, *CCND2* and *CDK6* expression (Fig. S3A), reentered the cell cycle and gave rise to PBs[4]. At D6, two days after inhibition of PIM2, the S-phase decreased, and cells accumulated in G0/G1 (Fig. 3A and Fig. S3B). In parallel, the number of generated PBs decreased (Fig. 2E-F), regardless of effects on cell death as shown by the QVD-OPH condition (Fig. S3B-C). Moreover, after short exposure to PIMi (12 h) the decrease of S-phase was already observable in absence of effect on apoptosis (Fig. S3B-D). Altogether, these results suggest that PIM2 promotes the G1/S transition independently of the cell death induction. We next performed cell cycle synchronization experiments in the XG21 MM cell line. As expected, unlike the control conditions – in which cells reached the S phase 6 h after release, PIM2 inhibition was associated with blockage of the cells in G1 (Fig. S3E).

The phosphatase CDC25A is required for the G1/S transition[22]. *CDC25A* gene expression was significantly greater in PBs than in CD23^{+} aBCs, as well as the protein expression (Fig. 3B). Chemical inhibition of CDC25A first led to a dramatic decrease in the proportion of S-phase cells and then, ultimately, to a strong reduction in the number of generated PBs (Fig. S3F,G). Interestingly, PIM2 inhibition led to the decrease of CDC25A protein level in PBs without affecting *CDC25A* expression (Fig. 3B and Fig. S3H). At D4, the addition of PIMi to cycloheximide-treated cells accelerated

CDC25A's degradation (Fig. 3C and Fig. S3I), while in presence of MG-132, cells maintained CDC25A expression (Fig. 3D).

Cyclin-dependent kinase (CDK) inhibitor 1B ($p27^{Kip1}$, encoded by the *CDKN1B* gene) prevents progression to G1[23]. This effect is linked to $p27^{Kip1}$'s location in the nucleus; cells that enter the cell cycle show a cyclin D2-mediated nuclear export of $p27^{Kip1}$[24]. *CDKN1B* expression was significantly higher in PBs than in $CD23^+$ aBCs, while $p27^{Kip1}$ protein expression was lower and mainly located in the nucleus in $CD23^+$ aBCs (Fig. 3E). In addition, we detected the threonine 198-phopshorylated (p(Thr198)) form of $p27^{Kip1}$, predominantly expressed in PBs compared to CD23+ aBCs (Fig. 3E). These results prompted us to assess the half-life of $p27^{Kip1}$ in PBs *vs.* $CD23^+$ aBCs. Cycloheximide-treated PBs were more susceptible to $p27^{Kip1}$ proteasome-mediated degradation, as shown after the addition of MG-132 (Fig. 3F,G). Interestingly, in highly proliferative D4 B cells, endogenous immunoprecipitation (IP) of $p27^{Kip1}$ revealed the binding of PIM2, and short treatment by PIMi resulted to a time-dependent decrease of p(Thr198)-$p27^{Kip1}$ (Fig. 3H). PBs generated after PIM2 inhibition showed an increase of the global level of $p27^{Kip1}$ expression - independently to *CDKN1B* expression - particularly in the nucleus (Fig. 3I and Fig. S3J,K). In cycloheximide-treated PBs, the addition of PIMi stabilized $p27^{Kip1}$ (Fig. 3J and Fig S3L). Finally, PIMi-treated PBs showed a decrease of p(Thr198)-$p27^{Kip1}$ as well as a decrease of poly-ubiquitinylated forms of $p27^{Kip1}$ in presence of MG-132 (Fig. 3K,L and Fig. S3M).

Overall, PIM2 expression during PB differentiation promotes the G1/S transition in prePBs by stabilizing CDC25A phosphatase and increasing the degradation of cytoplasmic $p27^{Kip1}$ (Fig. 3M).

PIM2 hinders the execution of caspase 3-driven apoptosis

The most prominent changes during PB commitment are related to cell death/survival[4]. Indeed, in culture, the majority of B cells were dead on D6 (Fig. 4A). The pan-caspase inhibitor QVD-OPH rescued the cells from death with the exception of the PBs; the latter appeared to be protected from apoptosis, and despite an increase in *CASP3* gene expression (Fig. 4A,B). Investigations of the proteins produced by the various cell subsets in our differentiation model showed that PBs contained higher levels of anti-apoptotic phosphorylated BAD (pBAD) and XIAP (Fig. 4C,D)[9,10]. Consistent with this finding, IP of PIM2 revealed a binding on BAD most likely required prior to phosphorylation (Fig. 4E). In accordance with this finding and despite the elevation in levels of procaspase 3, PBs displayed low levels of caspase 3 autocatalytic activity and thus did not produce many active p19/p17 forms (as highlighted by lower levels of cleaved PARP) as P2/CD23^{+} cells did (Fig. 4F)[25]. Overall, PBs maintain caspase 9 in an inactivated state and XIAP protein remains protected from degradation (Fig. 4C-F)[26]. XIAP is thought to have a key role in PBs by inhibiting caspase 3 activation. Indeed, IP of caspase 3 and XIAP revealed XIAP's binding on p19/p17 fragments of caspase 3 (Fig. 4G), which impairs their catalytic activity on procaspase 3[27,28]. Lastly, the P2/CD23^{+} cells' complete degradation of PARP (Fig. 4F) showed that terminal B cell differentiation is associated with apoptosis if cells are not otherwise protected by the PB commitment. In PBs, PIM2 inhibition induced an increase in activated caspase 3 levels and thus a decrease in cell viability (Fig. 4H,I and Fig S4A). This effect was driven by (i) the strong mitochondrial depolarization due to the inhibition of pBAD, (ii) the production of cleaved caspase 9, (iii) the decrease in XIAP, (iv) the detection of the p17 fragment of caspase 3, and (v) PARP cleavage (Fig. 4J-L). Lastly, addition of the caspase 3 inhibitor Q-DEVD-OPH rescued the PBs from cell death (Fig. S4B).

Taken as a whole, these data show that PIM2 counteracts the activation of caspase 3 in PBs and thus promotes cell survival.

PIM2 stabilizes cytoplasmic p21^{Cip1} and promotes the latter's binding to caspase 3

Like p27^{Kip1}, nuclear p21^{Cip1} is a CDK inhibitor and inhibits entry into the S phase of the cell cycle[29]. PB commitment was associated with a significant increase in transcription of *CDKN1A* (which encodes p21^{Cip1}) and levels of p21^{Cip1} were markedly higher in PBs than in CD23^{+} aBCs (Fig. 5A). Surprisingly, p21^{Cip1} was essentially expressed in the cytoplasm, and endogenous IP experiments yielded a multiprotein complex in which p21^{Cip1} interacted with PIM2 and HSP90β (Fig. 5B,C). Moreover, PIM2 inhibition led to a dramatic decrease in cytoplasmic p21^{Cip1} without effect on either *CDKN1A* expression or nucleus relocalization (Fig. 5D and Fig. S5A,B). The addition of PIMi to cycloheximide-treated cells accelerated p21^{Cip1}'s degradation (Fig. 5E). Treatment with MG-132 induced a strong accumulation of p21^{Cip1}, and the addition of PIMi was associated with elevated poly-ubiquitinylated p21^{Cip1} (Fig. 5F,G). XG21 cells presented similar results (Fig. S5C-F). Collectively, these results show that PIM2 stabilizes p21^{Cip1} in PBs by promoting its binding to a cytoplasmic multiprotein complex and thus, prevents p21^{Cip1}'s proteasome-mediated degradation.

This PIM2-induced cytoplasmic stabilization of p21^{Cip1} prompted us to question the latter's role in PB commitment. As described previously for other cell types[30,31], we hypothesized that p21^{Cip1} interacts with procaspase 3. In fluorescence resonance energy transfer (FRET)[32] experiments on XG21 cells, we detected a p21^{Cip1}/procaspase 3 complex whose formation was abrogated by pretreatment of the cells with PIMi (Fig. 5H). IP experiments confirmed the presence of this complex in

PBs (Fig. 5I and Fig. S5G). To determine whether or not $p21^{Cip1}$ mediates apoptosis inhibition, we used siRNA to downregulate *CDKN1A* expression (Fig. S5H). On D6, the generated PBs were found to contain p17-forms of caspase 3 and cleaved PARP - confirming that apoptosis had taken place (Fig. 5J and S5I). Treatment with the small-molecule $p21^{Cip1}$ inhibitor UC2288 was associated with a dose-dependent decrease in cell viability, which was restored by treatment with the caspase 3 inhibitor Q-DEVD-OPH (Fig. 5K and Fig. S5J,K).

Taken as a whole, these findings show that in addition to its mitochondrial effects, PIM2 inhibits the execution of apoptosis by stabilizing cytoplasmic $p21^{Cip1}$, allowing the latter to bind to procaspase 3, and thus inhibiting the production of activated caspase 3 (Fig. 5L).

Mature plasma cells need PIM2 to inhibit the activation of caspase 3

Plasma cell maturation is a continuum that runs from PBs to fully mature, long-lived PCs such as those residing in the bone marrow (BM) niche, where cell survival depends on various extrinsic factors[33]. A comparison of various tonsil-derived B cell populations, PBs, and BM PCs revealed that the level of *PIM2* expression increased along the maturation pathway (Fig. 6A). On paraffin-embedded BM biopsies, staining experiments revealed that virtually all BM PCs – detected either with CD138 or BCMA markers – were strongly positive for PIM2 (Fig. 6B and Fig. S6A,B).

To characterize the regulation and functional contribution of PIM2 in mature PCs, we adapted our cell culture model so that it produced non-proliferating $CD138^{+}$ PCs (Fig. S6C-F), in line with reports on an early PC (ePC) phenotype[34,35]. As was the case in BM PCs, high levels of PIM2 mRNA and protein expression were observed in ePCs (Fig. 6C). This expression was driven by IL-6 via STAT3 signaling and by the

supernatant from a mesenchymal stromal cell culture (Fig. 6D). As expected, the addition of anti-IL-6 and anti-IL-6R antibodies to the cell culture prevented the induction of PIM2 (Fig. 6D). In this context, we observed clusters of $CD138^{+}/PIM2^{+}$ PCs in some areas on BM biopsies, close to CD41-positive megakaryocytes – cells known to produce large amounts of IL-6 and participating to PC BM niche (Fig. 6E)[33].

Treatment of ePCs with PIMi induced an elevation of activated caspase 3 levels, and immunoblot experiments confirmed the increase of mitochondrial depolarization and the execution of apoptosis (Fig. 6F,G). PIMi treatment also led to a significant decrease in $p21^{Cip1}$ levels (Fig. 6G). Interestingly, ePCs (like in some BM PCs) only expressed $p21^{Cip1}$ in the cytoplasm (Fig. 6H and Fig. S6G), and FRET experiments revealed that PIM2 interacted with $p21^{Cip1}$ as well as $p21^{Cip1}$ with caspase 3 (Fig. 6I).

Taken as a whole, our data show that PIM2 is still required in quiescent PCs to protect cells from caspase 3 activation; PIM2 acts at various levels and notably stabilizes cytoplasmic $p21^{Cip1}$.

BH3 mimetics and PIM2 inhibitors have synergistic effects in multiple myeloma

Although PIM2's involvement in MM has been recognized for over a decade, our present findings prompted us to further investigate PIM2's status in malignant PCs. Data from the DepMap Project showed that mRNA expression of *PIM2* (but not of *PIM1*) was elevated in MM cells compared to other tumour cells, whereas CRISPR screening showed a specific high PIM2 dependency score for malignant PCs (Fig. 7A,B and Fig. S7A). BM biopsies from MM patients revealed the intense, widespread expression of PIM2 (Fig. 7C). Data from the University of Arkansas' Total Therapy 2 (TT2) MM cohort showed the strongest *PIM2* expression levels in the high-risk molecular subgroups (Fig. S7B)[36]. An analysis of data from 765 patients in the

CoMMpass cohort showed that *PIM2* expression was significantly elevated in high-risk cytogenetic subgroups and low in low-risk subgroups (Fig. S7C)[37,38]. In addition, high PIM2 expression patients compared to the PIM2^{low} group had a worse survival probability (Fig. 7D). This is in line with sc-RNA-seq data on malignant PCs from patients resistant to carfilzomib-daratumumab combination therapy which presented higher *PIM2* expression (Fig. S7D)[39]. Likewise, we observed a significant increase in *PIM2* expression in cells from an in-house cohort of 14 patients with disease progression soon after first-line treatment (Fig. S7E). Collectively, these data suggest that the severity of MM is associated with PIM2 expression levels.

Drug resistance is the greatest challenge in MM. It might be possible to overcome this obstacle by acting at the mitochondrial level and lowering the threshold for triggering mitochondrial apoptosis[40]. Venetoclax is reportedly effective in BCL2-translocated MM patients[41]. Furthermore, MCL1 is also an attractive target in MM[41,42] because of its essential effects on PCs survival via inactivation of the pro-apoptotic multidomain of BAX and BAK effectors[43]. However, in contrast to BCL2 and BCL-xL, MCL1's activity is not antagonized by BAD[44]. Interestingly, data from the TT2 MM cohort showed that the expression levels of MCL1 and PIM2 are significantly correlated (Fig. S7F). We hypothesized that targeting both PIM2 and MCL1 might have synergistic effects on mitochondria depolarization because the two proteins act at different levels (Fig. 7E). To this end, we first evaluated the respective effects of PIMi[45], an MCL1 inhibitor (AZD5991, referred to hereafter as MCL1i)[46] alone and then when combined. The XG7 and RPMI8226 cell lines were sensitive to MCL1i but the U266 cells were not (Fig. S7G). Low-dose treatment with PIMi greatly enhanced the response to MCL1i in XG7 and RPMI8226 cells (Fig. 7F and Fig. S7H). Interestingly, U266 cells (resistant to PIMi alone and MCL1i alone) became sensitive when the drugs were

combined (Fig. 7G). Lastly, PIMi and MCL1i had synergistic effects on primary MM cells from six patients without effect on $CD138^-$ cells (Fig. 7H).

Taken as a whole, these results confirmed that the mitochondrial control of PIM2 is similar in normal and malignant PCs; this finding opens up novel treatment options in MM.

DISCUSSION

The processes by which committed B cells and nascent PBs switch from one molecular program to another had not previously been fully characterized. Here, our experiments with human primary B cells demonstrated that PIM2 kinase is a pivotal factor for the generation and maintenance of PB and PC populations. In particular, our results showed how committed B cells reenter the cell cycle after their proliferation burst, and under subsequently restricted culture conditions, express high levels of PIM2 and thus decrease mitochondrial apoptosis.

Our molecular characterization provided strong evidence of the regulation of *PIM2* gene expression and demonstrates *PIM2*'s status as a true PC-identity gene recruited at the same time as *PRDM1* and *IRF4*, once BACH2 repression has been released. In prePBs and PBs, both IL-10 and IL-21 cytokines drive PIM2 expression via pSTAT3 signaling and (in PCs) by IL-6, which establishes a direct link between growth-factor-induced transcription and a kinase-dependent pathway that promotes survival and cell cycle reentry.

The cell cycle provides windows of opportunity for chromatin remodeling and thus gene activation[47]. Committed B cells increase their expression of *CDC25A* and in parallel PIM2 helps to stabilize the CDC25A protein and thus prompts cells to enter the S phase and progress to the PB state independently of effects on apoptosis[22]. Interestingly, PIM2's promotion of cell cycle is accentuated by the degradation of cytoplasmic $p27^{Kip1}$, which prevents the latter from accumulating or returning to the nucleus. Indeed, PIM2's effect on $p27^{Kip1}$ is mediated by the phosphorylation of threonine 198 residue, consistent with the known cytoplasmic localization of p(Thr198)-$p27^{Kip1}$ and its binding to 14-3-3 leading to its proteasomal degradation[48]. In contrast, in PCs, $p27^{Kip1}$ accumulated in the nucleus - independently of high PIM2 expression - to halt the cell cycle and so without being degraded by cytoplasmic PIM2.

Caspases 9 and 3 become resistant to activation by apoptotic stimuli when B cells differentiate into PBs, and the apoptosis of short-lived PCs *in vitro* and *in vivo* is largely independent of the key apoptotic caspases[49]. Our present results provide insights into the mechanisms whereby B cell death is avoided - despite intense expression of cell death-related genes in committed cells[4] - allowing PB generation and survival. Production of pBAD helps to maintain the integrity of mitochondria, as evidenced by increased XIAP expression and the overall inhibition of caspase 3 self-activation. Knockdown and dose-dependent experiments have shown that this mitochondrial adaptation is mediated and made possible by high levels of PIM2 expression and its binding activity to BAD; this is in line with data from constitutive PIM2 expression models, with the detection of pBAD, its binding to 14-3-3, and inhibition of BAD/BCL-XL binding[10,50].

One of the ways in which PIM2 regulates apoptosis during the differentiation of B cells into PBs involves restricting $p21^{Cip1}$ to the cytoplasm. During this step, cells progress

from G1 to S and proliferate; hence, the cytoplasmic expression of $p21^{Cip1}$ makes sense because its presence in the nucleus blocks cells in G1[51]. However, further investigations on quiescent PC populations demonstrate that $p21^{Cip1}$ stays in the cytoplasm which sheds light on its pleotropic functions. In PBs, PIM2 stabilizes cytoplasmic $p21^{Cip1}$ by promoting the formation of a complex with HSP90β and thus reducing the proteasomal degradation of $p21^{Cip1}$. Interestingly, $p21^{Cip1}$ also binds to procaspase 3 in a PIM2-dependent manner and FRET experiments showed that the addition of PIMi abrogated $p21^{Cip1}$'s binding to procaspase 3. In PBs, PIM2 acts by promoting the formation of a multiprotein complex which inhibits the caspase 3 activation. This effect complements the production of pBAD and the inhibition of mitochondrial depolarization and shows that PIM2 acts in several ways to ensure the survival of PBs.

Entry into cell cycle quiescence accompanies the final phenotypic maturation of PCs and requires CDK inhibitors regulated by IL-6[52]. By modifying the culture conditions, we obtained fully mature PCs that strongly expressed PIM2 and absolutely required IL-6. At the cellular level, PIM2's anti-apoptotic effects were characterized by maintenance of mitochondrial integrity and promotion of caspase 3/$p21^{Cip1}$ binding. Although it is now accepted that viability is not an intrinsic property of BM PCs but is conferred on the cells by their immediate environment[53], our present observations of marked expression of PIM2 in BM PCs suggest that this kinase has a crucial role in long-term cell survival and might be involved in the functional activity of the PC niche through IL-6-dependent crosstalk between the cell and its microenvironment[54].

Our results revealed a hitherto unexpected role of PIM2 kinase in terminal B cell differentiation and, more generally, the PC's biology. PIM2 kinase's pleotropic effects

enable the cell to modify its regulation of apoptosis and to promote survival when faced with protein secretion overload. The data from the DepMap Project show that malignant PCs are “addicted” to PIM2, and elevated PIM2 expression in the most severe cases of MM suggests that PIM2 is linked to clinical severity. Small-molecule inhibitors of PIM have given some encouraging results in preclinical models, and recently in MM patients with relapsed and/or refractory disease[55]. Indeed, and despite a relative low objective response rate (partial response or better), patients who reached the recommended dose of treatment, PIM447 drug demonstrated a single-agent antitumor activity with a significant improvement of the median progression-free survival and the rate of clinical benefit. However, bone marrow examination of patients failed to reveal a clinically significant reduction in malignant PCs suggesting that PIM447 exerted antitumor responses via cytostatic rather than apoptotic mechanisms[55]. Taking into account that MM tumor cells increase their dependence on MCL1 during the course of the disease[41], we could speculate that MCL1 could counteract the induction of cell death by PIMi. In the context of the PIM447 clinical trial[55], antiproliferative effects could appear at low doses while cell death would require dose escalation – possibly with unacceptable toxicities – to counterbalance MCL1-dependency. Given that MCL1’s action on the mitochondrial membrane is independent of BAD, dual pharmacological inhibition of PIM2 and MCL1 is highly synergistic; low doses of PIMi significantly increased the efficacy of the anti-MCL1 drug. Interestingly, this drug combination can reverse U266 cell’s primary resistance to MCL1i and PIMi.

In conclusion, our present results showed that the final transcriptional modifications in B cells committed to differentiation into PBs are associated with the expression of a set of crucial genes, including *PIM2*. The newly established adaptive status of the

generated PBs is maintained in mature PCs. Lastly, we showed that PIM2 kinase's anti-apoptotic effects should be further investigated in the context of novel treatment strategies in MM.

ACKNOWLEDGMENTS

This work was funded by an internal grant from the Hematology Laboratory, CHU de Rennes, and Région GO Ligue contre le Cancer. MH has received a doctoral fellowship from FHU CAMIn, Ligue Contre le Cancer/Comité d'Ile et Vilaine. AP received a PhD fellowship from Région Bretagne and Ligue Nationale contre le Cancer. Immunofluorescence studies were performed at the Microscopy Rennes Imaging Center (MRic-ALMF) and in the H2P2 facility, both of which are members of the UMS 6480 Biosit (Rennes, France) and the French national France-BioImaging infrastructure network funded by the French Research Agency (ANR-10-INBS-04). Cell sorting was performed at the Biosit Flow Cytometry and the CytomeTRI cell sorting facilities (UMS6480 Biosit). We are indebted to the Centre de Ressources Biologiques (CRB)-Santé (BB-0033-00056, http://www.crbsante-rennes.com) at Rennes University Medical Center for its help with processing biological samples, and we also thank several clinicians and patients for providing samples for research purposes. We thank the MMRF for sharing the RNA sequencing and clinical data for patients enrolled in the CoMMpass study via the MMRF genomics portal.

AUTHOR CONTRIBUTIONS

M.H. designed and conducted the experiments, and wrote the paper; G.C. designed the cell differentiation model, and performed cytometry and cell-sorting; F.C. performed genomic analysis; E.A performed ChIP-qPCR STAT3 experiments; J.D. performed

drug combination experiments; A.P. performed single-cell qPCRs; C.D. helped with BACH2 assays and discussed results; S.M. performed CDC25A immunoblotting; G.B. performed FRET experiments; R.V. performed immunostaining; F.L-G. provided bone marrow biopsies; A.M. designed morpholino SSO; O.D. provided multiple myeloma samples; K.T. discussed results; L.D. provided the antisense strategy; J.M. provided cell lines and original data; T.F. designed and supervised the experiments, and wrote the paper.

COMPETING INTERESTS

M.H., G.C., A.M., L.D., J.M. and T.F. have applied for a European patent on the use of an SSO to modulate PIM2 expression. The other authors have no conflicts of interest to declare.

REFERENCES

1. Fairfax KA, Kallies A, Nutt SL, Tarlinton DM. Plasma cell development: From B-cell subsets to long-term survival niches. *Seminars in Immunology*. 2008;20(1):49–58.

2. Willis SN, Nutt SL. New players in the gene regulatory network controlling late B cell differentiation. *Current Opinion in Immunology*. 2019;58:68–74.

3. Shaffer AL, Young RM, Staudt LM. Pathogenesis of Human B Cell Lymphomas. *Annu Rev Immunol*. 2012;30(1):565–610.

4. Caron G, Hussein M, Kulis M, et al. Cell-Cycle-Dependent Reconfiguration of the DNA Methylome during Terminal Differentiation of Human B Cells into Plasma Cells. *Cell Reports*. 2015;13(5):1059–1071.

5. Pignarre A, Chatonnet F, Caron G, et al. Plasmablasts derive from CD23– activated B cells after the extinction of IL-4/STAT6 signaling and IRF4 induction. *Blood*. 2021;137(9):1166–1180.

6. Mondello P, Cuzzocrea S, Mian M. Pim kinases in hematological malignancies: where are we now and where are we going? *J Hematol Oncol*. 2014;7:95–103.

7. Keane NA, Reidy M, Natoni A, Raab MS, O'Dwyer M. Targeting the Pim kinases in multiple myeloma. *Blood Cancer Journal*. 2015;5(7):e325–e325.

8. Panchal NK, Sabina EP. A serine/threonine protein PIM kinase as a biomarker of cancer and a target for anti-tumor therapy. *Life Sciences*. 2020;255:117866.

9. Fox CJ. The serine/threonine kinase Pim-2 is a transcriptionally regulated apoptotic inhibitor. *Genes Dev*. 2003;17(15):1841–1854.

10. Yan B, Zemskova M, Holder S, et al. The PIM-2 Kinase Phosphorylates BAD on Serine 112 and Reverses BAD-induced Cell Death. *J Biol Chem*. 2003;278(46):45358–45367.

11. Moreaux J, Klein B, Bataille R, et al. A high-risk signature for patients with multiple myeloma established from the molecular classification of human myeloma cell lines. *Haematologica*. 2011;96(4):574–582.

12. Greco WR, Bravo G, Parsons JC. The search for synergy: a critical review from a response surface perspective. *Pharmacol Rev*. 1995;47(2):331.

13. Combès E, Andrade AF, Tosi D, et al. Inhibition of Ataxia-Telangiectasia Mutated and RAD3-Related (*ATR*) Overcomes Oxaliplatin Resistance and Promotes Antitumor Immunity in Colorectal Cancer. *Cancer Res*. 2019;79(11):2933–2946.

14. Le Gallou S, Caron G, Delaloy C, et al. IL-2 Requirement for Human Plasma Cell Generation: Coupling Differentiation and Proliferation by Enhancing MAPK-ERK

Signaling. *J Immunol*. 2012;189(1):161–173.

15.Andersson R, Gebhard C, Miguel-Escalada I, et al. An atlas of active enhancers across human cell types and tissues. *Nature*. 2014;507(7493):455–461.

16.Hnisz D, Abraham BJ, Lee TI, et al. Super-Enhancers in the Control of Cell Identity and Disease. *Cell*. 2013;155(4):934–947.

17.Hipp N, Symington H, Pastoret C, et al. IL-2 imprints human naive B cell fate towards plasma cell through ERK/ELK1-mediated BACH2 repression. *Nat Commun*. 2017;8(1):1443–1426.

18.Ozaki K, Spolski R, Ettinger R, et al. Regulation of B Cell Differentiation and Plasma Cell Generation by IL-21, a Novel Inducer of Blimp-1 and Bcl-6. *J Immunol*. 2004;173(9):5361–5371.

19.Doody GM, Care MA, Burgoyne NJ, et al. An extended set of PRDM1/BLIMP1 target genes links binding motif type to dynamic repression. *Nucleic Acids Research*. 2010;38(16):5336–5350.

20.Shaffer AL, Lin K-I, Kuo TC, et al. Blimp-1 Orchestrates Plasma Cell Differentiation by Extinguishing the Mature B Cell Gene Expression Program. *Immunity*. 2002;17(1):51–62.

21.Minnich M, Tagoh H, Bönelt P, et al. Multifunctional role of the transcription factor Blimp-1 in coordinating plasma cell differentiation. *Nat Immunol*. 2016;17(3):331–343.

22.Hoffmann I, Draetta G, Karsenti E. Activation of the phosphatase activity of human cdc25A by a cdk2-cyclin E dependent phosphorylation at the G1/S transition. *Embo J*. 1994;13(18):4302–4310.

23.Abbastabar M, Kheyrollah M, Azizian K, et al. Multiple functions of p27 in cell cycle, apoptosis, epigenetic modification and transcriptional regulation for the control of cell growth: A double-edged sword protein. *DNA Repair*. 2018;69:63–72.

24.Susaki E, Nakayama K, Nakayama KI. Cyclin D2 Translocates p27 out of the Nucleus and Promotes Its Degradation at the G0-G1 Transition. *Mol Cell Biol*. 2007;27(13):4626–4640.

25.Ponder KG, Boise LH. The prodomain of caspase-3 regulates its own removal and caspase activation. *Cell Death Disc*. 2019;5(1):56–66.

26.Datta SR, Ranger AM, Lin MZ, et al. Survival Factor-Mediated BAD Phosphorylation Raises the Mitochondrial Threshold for Apoptosis. *Dev Cell*. 2002;3(5):631–643.

27.Riedl SJ, Renatus M, Schwarzenbacher R, et al. Structural Basis for the Inhibition of Caspase-3 by XIAP. *Cell*. 2001;104:791–800.

28.Suzuki Y, Nakabayashi Y, Nakata K, Reed JC, Takahashi R. X-linked Inhibitor of Apoptosis Protein (XIAP) Inhibits Caspase-3 and -7 in Distinct Modes. *J Biol Chem*. 2001;276(29):27058–27063.

29.Elledge SJ, Hardy CFJ, Pautz A, et al. Cell Cycle Checkpoints: Preventing an Identity Crisis. *Science*. 1996;274(5293):1964–1972.

30.Asada M. Apoptosis inhibitory activity of cytoplasmic p21Cip1/WAF1 in monocytic differentiation. *Embo J*. 1999;18(5):1223–1234.

31.Suzuki A, Kawano H, Hayashida M, et al. Procaspase 3/p21 complex formation to resist Fas-mediated cell death is initiated as a result of the phosphorylation of p21 by protein kinase A. *Cell Death Differ*. 2000;7(8):721–728.

32.Bertolin G, Sizaire F, Déméautis C, et al. Optimized FRET Pairs and Quantification Approaches To Detect the Activation of Aurora Kinase A at Mitosis. *ACS Sens.* 2019;4(8):2018–2027.

33.Winter O, Moser K, Mohr E, et al. Megakaryocytes constitute a functional component of a plasma cell niche in the bone marrow. *Blood*. 2010;116(11):1867–1875.

34.Kassambara A, Rème T, Jourdan M, et al. GenomicScape: An Easy-to-Use Web Tool for Gene Expression Data Analysis. Application to Investigate the Molecular Events in the Differentiation of B Cells into Plasma Cells. *PLoS Comput Biol*. 2015;11(1):e1004077.

35.Nutt SL, Hodgkin PD, Tarlinton DM, Corcoran LM. The generation of antibody-secreting plasma cells. *Nat Rev Immunol*. 2015;15(3):160–171.

36.Zhan F, Huang Y, Colla S, et al. The molecular classification of multiple myeloma. *Blood*. 2006;108(6):2020–2028.

37.Bergsagel PL, Mateos M-V, Gutierrez NC, Rajkumar SV, San Miguel JF. Improving overall survival and overcoming adverse prognosis in the treatment of cytogenetically high-risk multiple myeloma. *Blood*. 2013;121(6):884–892.

38.Perrot A, Lauwers-Cances V, Tournay E, et al. Development and Validation of a Cytogenetic Prognostic Index Predicting Survival in Multiple Myeloma. *J Clin Oncol*. 2019;37(19):1657–1665.

39.Cohen YC, Zada M, Wang S-Y, et al. Identification of resistance pathways and therapeutic targets in relapsed multiple myeloma patients through single-cell sequencing. *Nat Med*. 2021;27(3):491–503.

40.Gimenez-Bonafe P, Tortosa A, Perez-Tomas R. Overcoming Drug Resistance by Enhancing Apoptosis of Tumor Cells. *Current Cancer Drug Targets*. 2009;9(3):320–

340.

41.Gomez-Bougie P, Maiga S, Tessoulin B, et al. BH3-mimetic toolkit guides the respective use of BCL2 and MCL1 BH3-mimetics in myeloma treatment. *Blood*. 2018;132(25):2656–2669.

42.Slomp A, Moesbergen LM, Gong J, et al. Multiple myeloma with 1q21 amplification is highly sensitive to MCL-1 targeting. *Blood Advances*. 2019;3(24):4202–4214.

43.Peperzak V, Vikström I, Walker J, et al. Mcl-1 is essential for the survival of plasma cells. *Nat Immunol*. 2013;14(3):10.

44.Wei AH, Roberts AW, Spencer A, et al. Targeting MCL-1 in hematologic malignancies: Rationale and progress. *Blood Reviews*. 2020;44:100672.

45.Keeton EK, McEachern K, Dillman KS, et al. AZD1208, a potent and selective pan-Pim kinase inhibitor, demonstrates efficacy in preclinical models of acute myeloid leukemia. *Blood*. 2014;123(6):905–913.

46.Tron AE, Belmonte MA, Adam A, et al. Discovery of Mcl-1-specific inhibitor AZD5991 and preclinical activity in multiple myeloma and acute myeloid leukemia. *Nat Commun*. 2018;9(1):5341.

47.Pop R, Shearstone JR, Shen Q, et al. A Key Commitment Step in Erythropoiesis Is Synchronized with the Cell Cycle Clock through Mutual Inhibition between PU.1 and S-Phase Progression. *PLoS Biol*. 2010;8(9):e1000484.

48.Fujita N, Sato S, Katayama K, Tsuruo T. Akt-dependent Phosphorylation of p27Kip1Promotes Binding to 14-3-3 and Cytoplasmic Localization. *Journal of Biological Chemistry*. 2002;277(32):28706–28713.

49.Auner HW, Beham-Schmid C, Dillon N, Sabbattini P. The life span of short-lived plasma cells is partly determined by a block on activation of apoptotic caspases acting in combination with endoplasmic reticulum stress. *Blood*. 2010;116(18):3445–3455.

50.Macdonald A, Campbell DG, Toth R, et al. Pim kinases phosphorylate multiple sites on Bad and promote 14-3-3 binding and dissociation from Bcl-XL. *BMC Cell Biology*. 2006;7:1–14.

51.Kreis, Louwen, Yuan. The Multifaceted p21 (Cip1/Waf1/CDKN1A) in Cell Differentiation, Migration and Cancer Therapy. *Cancers*. 2019;11(9):1220.

52.Tourigny MR, Ursini-Siegel J, Lee H, et al. CDK Inhibitor p18INK4c Is Required for the Generation of Functional Plasma Cells. *Immunity*. 2002;17(2):179–189.

53.Sze DM-Y, Toellner K-M, de Vinuesa CG, Taylor DR, MacLennan ICM. Intrinsic Constraint on Plasmablast Growth and Extrinsic Limits of Plasma Cell Survival. *J Exp Med*. 2000;192(6):813–822.

54.Wols HAM, Underhill GH, Kansas GS, Witte PL. The Role of Bone Marrow-Derived Stromal Cells in the Maintenance of Plasma Cell Longevity. *J Immunol*. 2002;169(8):4213–4221.

55.Raab MS, Thomas SK, Ocio EM, et al. The first-in-human study of the pan-PIM kinase inhibitor PIM447 in patients with relapsed and/or refractory multiple myeloma. *Leukemia*. 2019;33(12):2924–2933.

56.Marchalot A, Lambert J-M, Boyer F, et al. Splice switching oligonucleotide mediated gene knockdown in B cells and plasma cells. *BioRvix preprint*. 2020;

57.Zammarchi F, de Stanchina E, Bournazou E, et al. Antitumorigenic potential of STAT3 alternative splicing modulation. *Proc Natl Acad Sci USA*. 2011;108(43):17779–17784.

FIGURE LEGENDS

Fig 1. PIM2 expression and regulation during normal B cell differentiation

A. Using a two-step cell culture process, VPD-labeled NBCs were differentiated into the cell populations P1, P2 and P3. P2 cells were subdivided into P2/CD23^{+} and P2/CD23^{-} subsets. The plasmablast P1 population arose from the P2/CD23- subset.

B. **Left**, *PIM2* RNA-seq results on D4 or D5 in the various cell populations. Data are quoted as the mean ± SD, n=3. **Right**, *PIM2* mRNA expression in the various cell populations on D6. mRNA data are quoted as the median (range), n=6. **Bottom**, PIM2 protein expression in all cell populations, from D0 to D6.

C. A single-cell qRT-PCR heatmap of the expression of 31 genes in P2/CD23^{-} vs. P2/CD23^{+} cell subsets; red arrow indicates *PIM2* mRNA expression.

D. *PIM2* mRNA expression (top) and protein expression (bottom) in different tonsil-derived B cell populations. mRNA data are quoted as the median (range), n=7.

E. The Integrative Genomic Viewer (IGV) genome browser window, showing several features around the *PIM2* locus. Colored tracks at the top are our RNA-seq and ATAC-seq data[5]. ATAC-seq showed that the open regions included the *PIM2* promoter and an upstream enhancer which physically interact together. ATAC-seq regions close to PIM2 comprise transcription factor binding sites (TFBS) for relevant factors such as STAT3, according to ENCODE data, and also BACH2, including one we have identified by chromatin immunoprecipitation[17]. 5hmC marks are identified in ATAC-seq regions and the body of the *PIM2* sequence in PBs[4]. For details, see Fig. S2a.

F. Levels of *BACH2* and *PIM2* mRNA expression (left) and protein expression (right) in D4^{lo} cells after transfection with siBACH2 on D2. mRNA data are quoted as the mean ± SD, n=4.

G. On D5, PBs were sorted, starved and then stimulated with the indicated cytokines. **Left**, *PIM2* mRNA expression after 4 h (white) and 16 h (black). For each time point, the results were normalized against the non-stimulated condition (set arbitrarily to 1, in grey). mRNA data are quoted as the mean ± SD, n=5. **Right**, PIM2, pSTAT3 and pSTAT5 protein expression after 16 h.

H. On D5, PBs were sorted, starved and then treated with increasing doses of a STAT3 inhibitor 1 h before the addition of IL-10. *PIM2* mRNA expression (left) and protein expression (right) were assessed 4 h after the addition of IL-10. mRNA data are quoted as the mean ± SD, n=5.

J. Regulation of PIM2 expression during B cell differentiation. At the start of B cell differentiation and despite the open chromatin on the promoter and on other regulatory regions, *PIM2* expression is constrained by BACH2. BACH2 expression then declines throughout the differentiation process, while T follicular helper (Tfh)-driven molecules stimulate STAT3 signaling. Both events promote the burst in PIM2 expression in cells committed to differentiation into PBs.

C, F, G, H, Statistical significance was evaluated using Mann-Whitney (**C, F, G, H**) or Kruskal-Wallis (**H**) test. **P* < 0.05, ***P* < 0.01, ****P* < 0.001.

See also Fig. S1.

Fig 2. Specific inhibition of PIM2 affects the generation of plasmablasts

A. **Left,** On D6, total blood B cells were differentiated into two different cell populations: CD23+ aBCs and PBs. **Right,** *PIM2* mRNA expression and protein expression in CD23+ aBCs and PBs on D6. Data are quoted as the median (range), n=10.

B. Diagram illustrating the SSO-PIM2's mode of action. Specific inhibition of PIM2

was perform by specifically blocking *PIM2* gene expression using a novel antisense RNA strategy based on a morpholino splice-switching oligonucleotide (SSO). In line with a previously described forced-splicing-dependent nonsense-mediated decay approach to knockdown[56,57], the SSO targets the 5' splice site of *PIM2*'s exon 2, induces out-of-frame exon skipping, and generates a premature stop codon in exon 4. This latter eventually triggers nonsense-mediated decay or generates a truncated, non-functional protein. See the Supplementals Materiel & Methods for details.

C. Activated B cells were treated with various doses of SSO-PIM2 from D4 to D6. **Top,** *PIM2* mRNA expression levels were compared with those in a control experiment, set arbitrarily to 100% (mean ± SD, n=4) (top). The agarose gel from the *PIM2* PCR shows the exon skipping (bottom). Dose escalation experiments allow us to select an SSO-PIM2 concentration of 2 µM for our subsequent experiments in our in vitro model. **Bottom,** PIM2 protein expression was assessed by western blot on D6 after PIM2 inhibition with increasing dose of SSO-PIM2.

D. *PIM2* mRNA expression (mean ± SD, n=6) (left) and protein expression (right), as determined by immunoblotting and immunofluorescence in CD23+ aBCs and PBs after PIM2 inhibition with SSO-PIM2 (2 µM). Sytox (blue) stains the nucleus. Scale bar: 10 µm.

E-F. On D4, cells were treated with SSO-PIM2 (**E**) or increasing doses of PIMi (**F**). On D6, analysis of cell differentiation was performed in the model described in Fig. 2A. Proportion of CD23+ aBCs ($CD23^{+}/CD38^{low}$ cells) and PBs ($CD38^{high}/CD23^{-}$ cells), and the absolute number of each cell population were assessed by flow cytometry according to the gating strategy described in Fig. S2D". **Left**, the absolute number of PBs and CD23+ aBCs obtained on D6 after PIM2 inhibition, compared with controls. Data are quoted as the mean ± SD, n=8. **Right**, one representative result of

the proportion of PBs on D6 (evaluated using flow cytometry) after PIM2 inhibition, compared with controls.

A, E, F, Statistical significance was evaluated using Mann-Whitney (**A**), Wilcoxon (**E**) and Friedman (**F**) tests. *$P < 0.05$, **$P < 0.01$, ***$P < 0.001$, ****$P < 0.0001$.

See also Fig. S2.

Fig 3. PIM2 supports cell cycle entry by promoting the G1/S transition

A. Flow cytometry evaluation of the cell cycle in PBs on D6 after treatment with SSO-PIM2 and increasing doses of PIMi, compared with controls (n=6).

B. **Left,** *CDC25A* mRNA expression in CD23+ aBCs and PBs on D6. Data are quoted as the median (range), n=10. **Right,** CDC25A protein expression (in the red square) in CD23+ aBCs and PBs on D6 after treatment with PIMi . *) *non-specific band*.

C. D4 B cells were treated with PIMi and incubated with cycloheximide (CHX). At the indicated time points, CDC25A expression was analyzed by immunoblotting.

D. On D4, B cells were treated with PIMi and incubated in presence of MG-132 for 2 h. CDC25A expression was analyzed by immunoblotting.

E. **Left**, *CDKN1B* mRNA expression in CD23+ aBCs and PBs on D6. Data are quoted as the median (range), n=10. **Right**, PIM2, p(Thr198)-$p27^{Kip1}$ (p-p27) and total $p27^{Kip1}$ protein expression in CD23+ aBCs and PBs on D6 in total protein extracts and nuclear & cytoplasmic fractions.

F. Cells were incubated with cycloheximide (CHX) on D6, just before sorting. At the indicated time points, $p27^{Kip1}$ expression in CD23+ aBCs and PBs was analyzed by immunoblotting.

G. Cells were incubated for 4 h with MG-132 before sorting on D6. $p27^{Kip1}$ expression in CD23+ aBCs and PBs was assessed by immunoblotting.

H. Left, Immunoprecipitation of $p27^{Kip1}$ in D4-activated B cells. PIM2 and $p27^{Kip1}$ were detected by immunoblotting. **Right,** On D4, activated B cells were shortly treated with PIMi. At the indicated time points, p(Thr198)-$p27^{Kip1}$ (p-p27) and total $p27^{Kip1}$ protein expression were assessed by immunoblotting.

I. PIM2 and $p27^{Kip1}$ protein expression in PBs after treatment with PIMi in total protein extracts and nuclear & cytoplasmic fractions.

J. On D6, cells were treated with PIMi and incubated with CHX before sorting. At the indicated time points, $p27^{Kip1}$ expression in PBs was assessed by immunoblotting.

K. On D6, cells were treated with PIMi for 2 h before sorting. p(Thr198)-$p27^{Kip1}$ (p-p27) and total $p27^{Kip1}$ were assessed by immunoblotting.

L. On D6, cells were incubated in presence or absence of PIMi for 2 h before addition (or not) of MG-132 for 4 h. **Left,** $p27^{Kip1}$ was assessed by immunoblotting. **Right,** Polyubiquitinated $p27^{Kip1}$ and native $p27^{Kip1}$ were assessed by immunoblotting.

M. PIM2 promotes the G1/S transition. Positive effects (in pink) are PIM2-dependent, while effects not directly related to PIM2 are shown in green. On one hand, PIM2 induces $p27^{Kip1}$ degradation once the protein is localized in the cytoplasm. On the other hand, PIM2 maintains the expression of CDC25A.

A, B, E, Statistical significance was evaluated using Kruskal-Wallis (**A**, for PIMi experiment) and Mann-Whitney (**A**, for SSO experiment, **B, E**) tests. **P* < 0.05, ***P* < 0.01, ****P* < 0.001, *****P* < 0.0001, ns = not significant.

See also Fig. S3.

Fig 4. PIM2 is required to counter mitochondrial apoptosis.

A. Analysis of cell death was performed in the model previously described in[5]. Cell viability (number of caspase-3-active negative (alive cells) and positive (death cells))

and cell differentiation (number of P3 cells, P2/CD23+ cells, P2/CD23- cells and P1 cells) was assessed by flow cytometry. **Left**, the total numbers of dead cells and living cells in the four populations on D6. The pie chart shows the percentage of cells, n=7. **Right**, on D4, cells were treated (or not) with QVD-OPH. On D6, the numbers of cells in each population were recorded. Data are quoted as the mean ± SD, n=6.

B. *CASP3* mRNA expression in the various cell populations on D6. The data are quoted as the median (range), n=6.

C. Factors in the mitochondrial apoptosis pathway involved in B cell differentiation. The green "+" symbol represents a death-activating effect, while the red "-" symbol represents a death-inhibiting effect. The pro-apoptotic protein BAD causes depolarization of the mitochondria, followed by the cleavage of procaspase 9 into active caspase 9 which in turn cleaves procaspase 3 to generate an intermediate, inactive p20 form. Following an auto-catalytic process, the p20 form gives rise to catalytically active p19 and p17 fragments. These molecules cleave PARP (the end effector in the apoptotic process) and also p20 in a feedback loop. Molecules are released from the mitochondria following depolarization and block the action of the inhibitor of apoptosis proteins, including XIAP. The phosphorylation of BAD leads to its cytoplasmic sequestration by 14-3-3, thus hijacking its pro-apoptotic effect.

D, F. Assessment of the protein expression of factors involved in the mitochondrial apoptosis pathway during primary B cell differentiation. "*Cl" for cleaved.*

E. Immunoprecipitation of PIM2 in PBs. PIM2 and BAD were detected by immunoblotting.

G. Immunoprecipitation of XIAP (top) and caspase 3 (bottom) in PBs. XIAP and caspase 3 were detected by immunoblotting.

H-I. Flow cytometry evaluation of the percentage of active-caspase-3-positive PBs on

D6, after treatment with SSO-PIM2 (**H**) or with increasing doses of PIMi (**I**), relative to controls. Data are quoted as the mean ± SD, n=8.

J. One representative result of the TMRM signal on D6 in PBs (analyzed by flow cytometry) after treatment with SSO-PIM2 (left) or PIMi (right), compared with controls.

K-L. Assessment of protein expression levels in PBs on D6 for factors involved in the mitochondrial apoptosis pathway after PIM2 inhibition by SSO-PIM2 (**K**) or PIMi (10 µM) (**L**), compared with controls.

A, B, H, I, Statistical significance was evaluated using Mann-Whitney (**A, B**), Wilcoxon (**H**) and Friedman (**I**) tests. **P* < 0.05, ***P* < 0.01, ****P* < 0.001, *****P* < 0.0001, ns = not significant.

See also Fig. S4.

Fig 5. PIM2 helps to stabilize cytoplasmic p21^{Cip1} and promotes the caspase 3/p21^{Cip1} interaction

A. Left, *CDKN1A* mRNA expression was measured on D6 in CD23+ aBCs and PBs. Data are quoted as the median (range), n=10. **Right,** PIM2 and p21^{Cip1} protein expression on D6 in CD23+ aBCs and PBs.

B. PIM2 and p21^{Cip1} protein expression was measured in nuclear & cytoplasmic fractions from CD23+ aBCs and PBs.

C. PIM2 (left) and p21^{Cip1} (right) immunoprecipitation in PBs. HSP90β, p21^{Cip} and PIM2 were detected by immunoblotting.

D. PIM2 and p21^{Cip1} protein expression after treatment with SSO-PIM2 (top) or PIMi (bottom) in total extracts from PBs.

E. PBs were sorted and then treated with PIMi and incubated with CHX. At indicated

times, $p21^{Cip1}$ expression was assessed by immunoblotting.

F. PBs were sorted and then treated with PIMi for 2 h in presence (or not) of MG-132. $p21^{Cip1}$ was assessed by immunoblotting.

G. PBs were treated 30 min with PIMi after incubation in the presence of MG-132 for 2 h. Polyubiquitinated $p21^{Cip1}$ and native $p21^{Cip1}$ were assessed by immunoblotting.

H. FRET/FLIM was analyzed in XG21 cells stained for caspase 3 (the donor) in the presence or absence of $p21^{Cip1}$ (the acceptor). Cells were left untreated (upper panel) or treated with PIMi (lower panel). The graph shows the quantified ΔLifetime. Data are quoted as the median (range), n=20 cells per condition. Pseudocolor scale: pixel-by-pixel ΔLifetime. Scale bar: 10 µm.

I. $p21^{Cip1}$ (top) and caspase 3 (bottom) immunoprecipitation in PBs. Caspase 3 and $p21^{Cip}$ were detected by immunoblotting.

J. $p21^{Cip1}$, procaspase 3, cleaved caspase 3 and cleaved PARP protein expression on D6 in PBs, after transfection with siCDKN1A or siCTL on D4.

K. On D4, activated B cells were treated for 24 h with increased doses of p21i in the presence or absence of Q-DEVD-OPH. PB viability (the proportion of active-caspase-3-negative cells) was assessed by flow cytometry. Data are quoted as the mean ± SD, n=5.

L. The PIM2/$p21^{Cip1}$/caspase 3 pathway in PBs. $p21^{Cip1}$ is stabilized in the cytoplasm by a protein complex that also includes PIM2 and HSP90β. Due to this localization, $p21^{Cip1}$ interacts with procaspase 3 and blocks its activation.

A, H, K, Statistical significance was evaluated using Mann-Whitney (**A, H**) and Kruskal-Wallis (**K**) tests. **P* < 0.05, ***P* < 0.01, ****P* < 0.001, *****P* < 0.0001.

See also Fig. S5.

Fig 6. PIM2 in bone marrow plasma cells

A. *PIM2* mRNA expression in different tonsil-derived B cell populations (n=7) and in BM PCs (n=9). The data are quoted as the median (range).

B. Immunofluorescence staining of PIM2 (green) and CD138 (orange) on paraffin-embedded normal BM. DAPI (blue) stains the nucleus. Scale bar: 20 μm.

C. *PIM2* mRNA and PIM2 protein expression in CD23+ aBCs and PBs on D6 and ePCs on D10. Data are quoted as the median (range), n=10.

D. On D10, ePCs were sorted, starved and treated (or not) with an anti-R-IL6 mAb 1 h before stimulation. IL-6 and supernatants of BM mesenchymal stroma cells (s-MSC) were pre-incubated (or not) for 1 h with an anti-IL6 mAb. *PIM2* mRNA expression (left) and protein expression (right) in ePCs 5 h after the addition of IL-6 or s-MSC. Data are quoted as the mean ± SD, n=4.

E. Immunofluorescence staining of PIM2 (green), CD41 (red) and CD138 (orange) on paraffin-embedded normal BM. DAPI (blue) stains the nucleus. Scale bar: 20 μm.

F. On D9, cells were treated with PIMi. The proportion of active-caspase-3-positive cells was assessed on D10, using flow cytometry. Data are quoted as the mean ± SD, n=6.

G. On D10, live cells were treated for 2 h with PIMi. Protein expression levels of caspase 9, XIAP, caspase 3, and $p21^{Cip}$ were assessed by immunoblotting.

H. $p21^{Cip1}$ expression was assessed on D10 in nuclear & cytoplasmic fractions by immunoblotting and immunofluorescence. Sytox (blue) stains the nucleus. Scale bar: 5 μm.

I. FRET/FLIM data were analyzed for ePCs stained for (the donor) PIM2 (left) or caspase 3 (right) in the presence or absence of $p21^{Cip1}$ (the acceptor). The graph shows the quantified Δlifetime. Data are quoted as the median (range), n=20 cells per

condition. Pseudocolor scale: pixel-by-pixel Δlifetime. Scale bar: 10 μm.

A, C, D, F, I, Statistical significance was evaluated using Mann-Whitney test. **P* < 0.05, ***P* < 0.01, ****P* < 0.001, *****P* < 0.0001.

See also Fig S6.

Fig 7. Reconsideration of PIM2 as an effective target in multiple myeloma

A. *PIM2* gene expression in cell lines derived from various solid and blood cancers (https://depmap.org/portal/).

B. CRISPR screening data from the DepMap project show that PIM2 presents the highest dependency score for the 20 tested MM cell lines, relative to other cell lines.

C. Immunohistofluorescence staining of PIM2 (green) and CD138 (orange) in paraffin-embedded BM from MM patients. DAPI (blue) stains the nucleus. Scale bar: 20 μm (Top). Scale bar: 50 μm (Bottom).

D. Overall survival of patients from the CoMMpass cohort as a function of PIM2 expression (PIM-high group; n=539 and PIM-low group (n=227)). The expression cutoff was determined by applying the MaxStat package (cutoff = 313.02).

E. Effects of BH3-mimetics and PIMi on apoptosis. BH3-mimetics (such as MCL1i and venetoclax) inhibit the binding of anti-apoptotic molecules (MCL1 and BCL2, respectively) to the pro-apoptotic effectors BAK and BAX; this leads to mitochondrial depolarization and, ultimately, cell apoptosis. PIMi enhances BAD's action: BAD binds to BCL2 and BCL-XL and therefore acts independently of MCL1i. The combination of these two compounds might result in greater activation of BAX and BAK and might increase the likelihood of cell death.

F-G. Left, The results of a cell viability assay and a synergy analysis after treatment with increasing concentrations of AZD1208 (PIMi) and AZD5991 (MCL1i) in XG7 cells

(**F**) and U266 cells (**G**). **Right**, Flow cytometry assessment of apoptosis using DAPI/CaspGlow staining and immunoblotting for the detection of caspase 3 and PARP cleavage, after treatment of XG7 cells (**F**) and U266 cells (**G**) with selected doses of inhibitors. The bar plot shows the percentage of caspase-3-active positive cells. Data are quoted as the mean ± SD, n=5.

H. Flow cytometry assessment of viability for primary cells from six MM patients. The bar plot shows the percentage of viable $CD138^+$ MM cells and $CD138^-$ cells, relative to a control (set to 100%) after treatment with the selected doses of inhibitor.

F, G, H, Statistical significance was evaluated using Mann-Whitney test. $^{**}P < 0.01$.

See also Fig. S7.

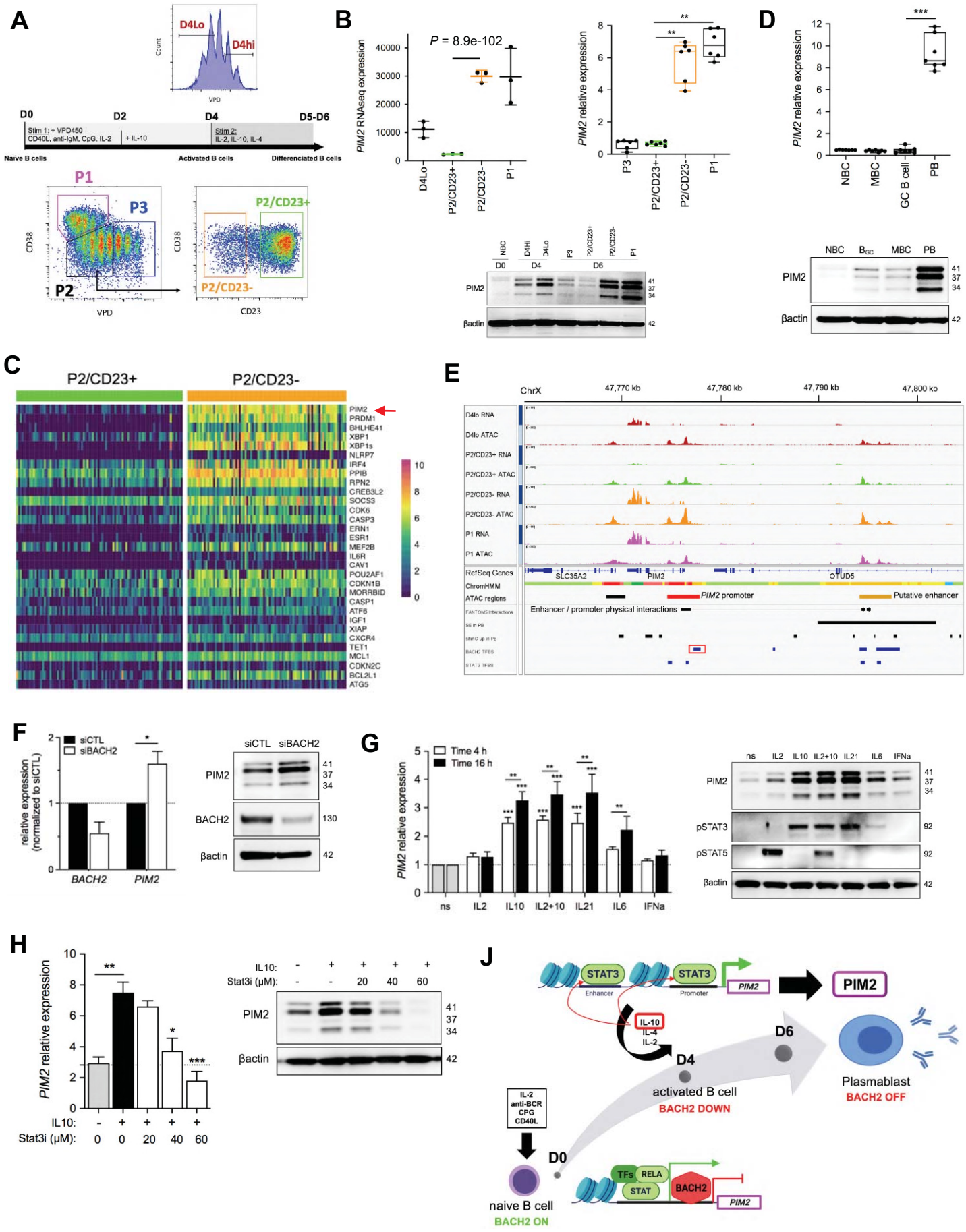

A
D4Lo
D4hi
Count
VPD
D0
D2
D4
D5-D6
Stim 1: + VPD450
CD40L, anti-IgM, CpG, IL-2
+ IL-10
Stim 2:
IL-2, IL-10, IL-4
Naïve B cells
Activated B cells
Differenciated B cells
P1
P3
P2
P2/CD23+
P2/CD23-
CD38
CD23
B
P = 8.9e-102
PIM2 RNAseq expression
D4Lo
P2/CD23+
P2/CD23-
P1
PIM2 relative expression
P3
D
PIM2 relative expression
NBC
MBC
GC B cell
PB
D0
D4
D6
PIM2
βactin
BGC
C
P2/CD23+
P2/CD23-
PIM2
PRDM1
BHLHE41
XBP1
XBP1s
NLRP7
IRF4
PPIB
RPN2
CREB3L2
SOCS3
CDK6
CASP3
ERN1
ESR1
MEF2B
IL6R
CAV1
POU2AF1
CDKN1B
MORRBID
CASP1
ATF6
IGF1
XIAP
CXCR4
TET1
MCL1
CDKN2C
BCL2L1
ATG5
E
ChrX
47,770 kb
47,780 kb
47,790 kb
47,800 kb
D4lo RNA
D4lo ATAC
P2/CD23+ RNA
P2/CD23+ ATAC
P2/CD23- RNA
P2/CD23- ATAC
P1 RNA
P1 ATAC
RefSeq Genes
ChromHMM
ATAC regions
SLC35A2
PIM2
OTUD5
PIM2 promoter
Putative enhancer
Enhancer / promoter physical interactions
F
siCTL
siBACH2
relative expression (normalized to siCTL)
BACH2
PIM2
BACH2
130
G
Time 4 h
Time 16 h
PIM2 relative expression
ns
IL2
IL10
IL2+10
IL21
IL6
IFNa
pSTAT3
pSTAT5
92
H
PIM2 relative expression
IL10:
Stat3i (μM):
0
20
40
60
J
STAT3
Enhancer
Promoter
PIM2
IL-10
IL-4
IL-2
D4
activated B cell
BACH2 DOWN
D6
Plasmablast
BACH2 OFF
IL-2
anti-BCR
CPG
CD40L
D0
naive B cell
BACH2 ON
TFs
RELA
STAT
BACH2

Fig. 1

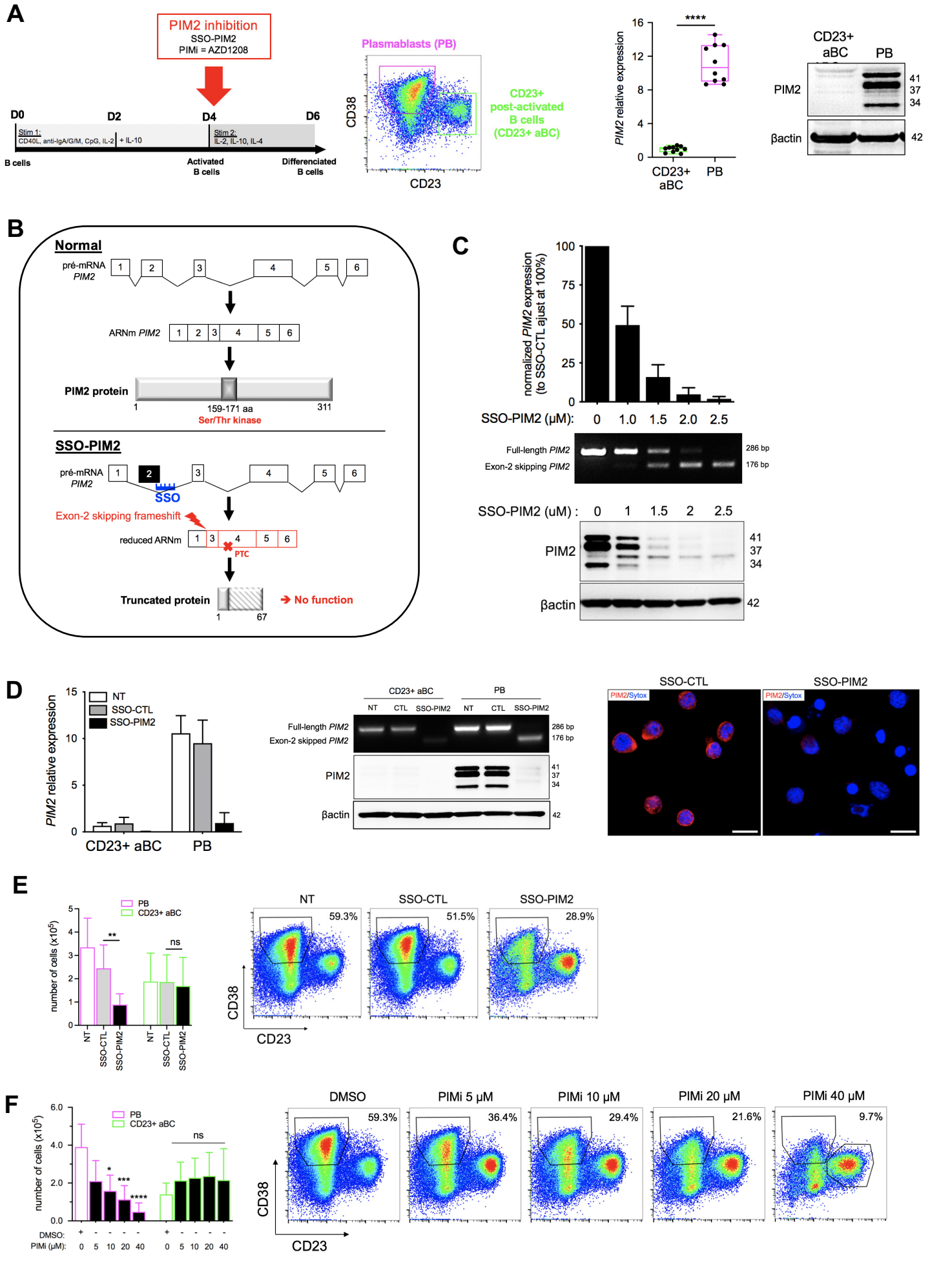

A
PIM2 inhibition
SSO-PIM2
PIMi = AZD1208
D0
D2
D4
D6
Stim 1:
CD40L, anti-IgA/G/M, CpG, IL-2
+ IL-10
Stim 2:
IL-2, IL-10, IL-4
B cells
Activated B cells
Differenciated B cells
Plasmablasts (PB)
CD38
CD23
CD23+ post-activated B cells (CD23+ aBC)
PIM2 relative expression
****
CD23+ aBC
PB
PIM2
βactin
41
37
34
42
B
Normal
pré-mRNA PIM2
ARNm PIM2
PIM2 protein
1
159-171 aa
311
Ser/Thr kinase
SSO-PIM2
SSO
Exon-2 skipping frameshift
reduced ARNm
PTC
Truncated protein
No function
67
C
normalized PIM2 expression (to SSO-CTL ajust at 100%)
SSO-PIM2 (μM): 0 1.0 1.5 2.0 2.5
Full-length PIM2
Exon-2 skipping PIM2
286 bp
176 bp
SSO-PIM2 (uM) : 0 1 1.5 2 2.5
D
PIM2 relative expression
NT
SSO-CTL
SSO-PIM2
CD23+ aBC
PB
Full-length PIM2
Exon-2 skipped PIM2
SSO-CTL
SSO-PIM2
PIM2/Sytox
E
number of cells (x10⁵)
**
ns
59.3%
51.5%
28.9%
F
DMSO
PIMi 5 μM
PIMi 10 μM
PIMi 20 μM
PIMi 40 μM
59.3%
36.4%
29.4%
21.6%
9.7%
DMSO:
PIMi (μM):

Fig. 2

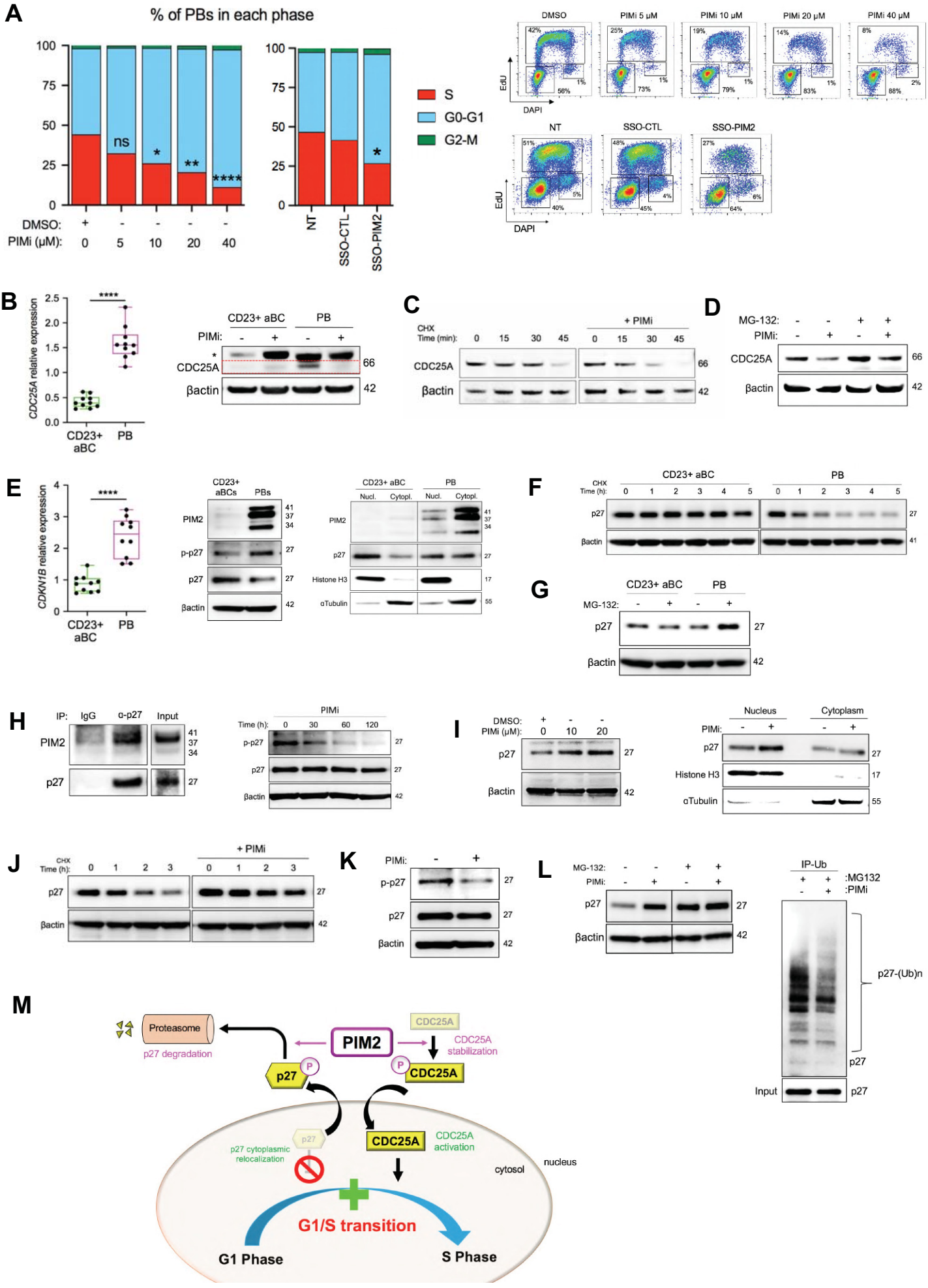

A
% of PBs in each phase
S
G0-G1
G2-M
DMSO:
PIMi (μM):
NT
SSO-CTL
SSO-PIM2
DMSO
PIMi 5 μM
PIMi 10 μM
PIMi 20 μM
PIMi 40 μM
EdU
DAPI
B
CDC25A relative expression
CD23+ aBC
PB
PIMi:
CDC25A
βactin
C
CHX
Time (min):
+ PIMi
D
MG-132:
E
CDKN1B relative expression
CD23+ aBCs
PBs
Nucl.
Cytopl.
PIM2
p-p27
p27
Histone H3
αTubulin
F
Time (h):
G
H
IP:
IgG
α-p27
Input
I
Nucleus
Cytoplasm
J
K
L
IP-Ub
:MG132
:PIMi
p27-(Ub)n
M
Proteasome
p27 degradation
PIM2
CDC25A
CDC25A stabilization
p27 cytoplasmic relocalization
CDC25A activation
cytosol
nucleus
G1/S transition
G1 Phase
S Phase

Fig. 3

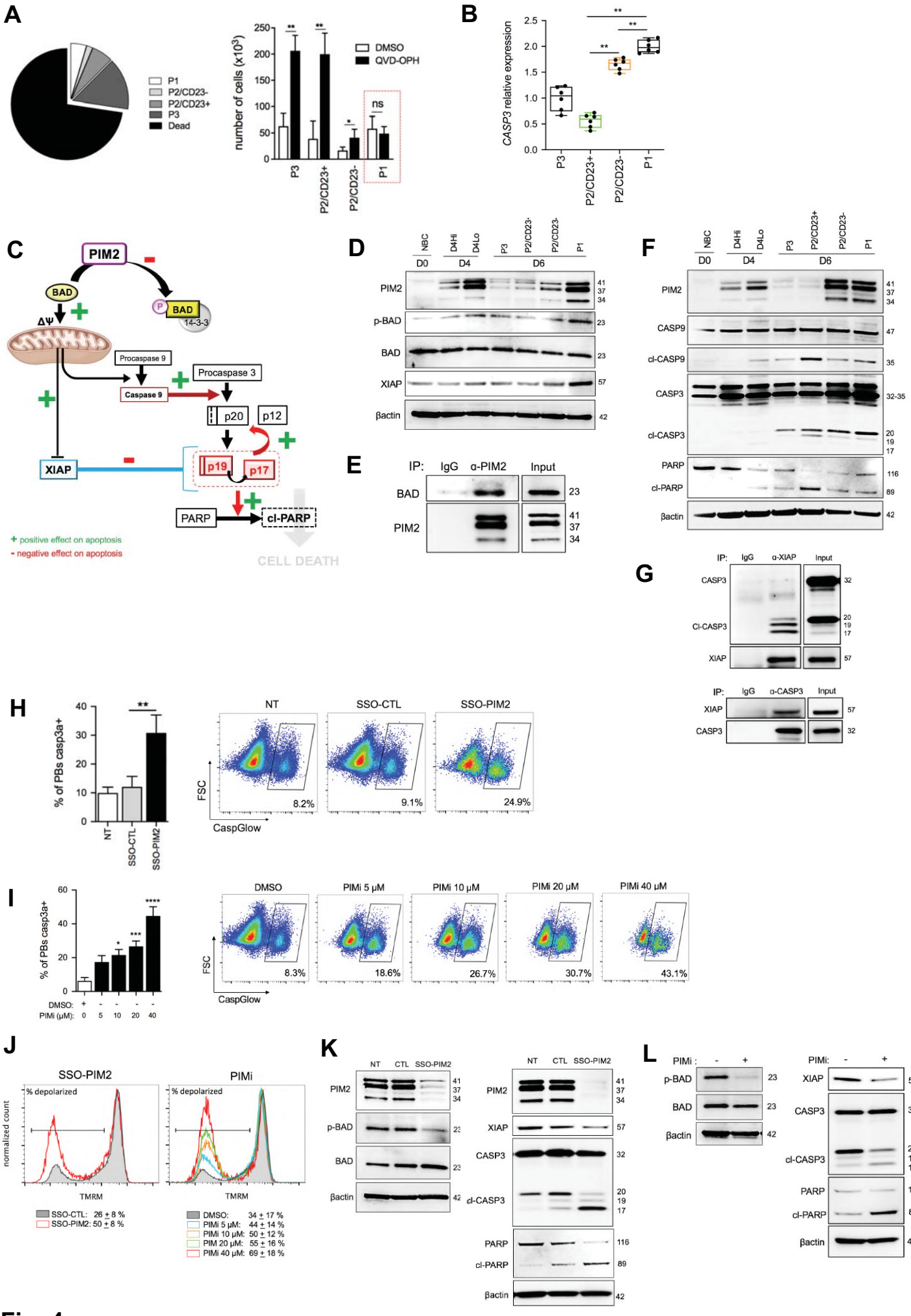

A
P1
P2/CD23-
P2/CD23+
P3
Dead
number of cells (x10³)
DMSO
QVD-OPH
ns
P3
P2/CD23+
P2/CD23-
P1
B
CASP3 relative expression
C
PIM2
BAD
ΔΨ
14-3-3
Procaspase 9
Caspase 9
Procaspase 3
p20
p12
XIAP
p19
p17
PARP
cl-PARP
CELL DEATH
+ positive effect on apoptosis
- negative effect on apoptosis
D
NBC
D4Hi
D4Lo
D0
D4
D6
PIM2
p-BAD
BAD
XIAP
βactin
E
IP: IgG α-PIM2 Input
F
CASP9
cl-CASP9
CASP3
cl-CASP3
PARP
cl-PARP
G
IP: IgG α-XIAP Input
IP: IgG α-CASP3 Input
H
% of PBs casp3a+
NT
SSO-CTL
SSO-PIM2
FSC
CaspGlow
8.2%
9.1%
24.9%
I
DMSO
PIMi 5 µM
PIMi 10 µM
PIMi 20 µM
PIMi 40 µM
8.3%
18.6%
26.7%
30.7%
43.1%
DMSO:
PIMi (µM):
J
SSO-PIM2
PIMi
% depolarized
normalized count
TMRM
SSO-CTL: 26 ± 8 %
SSO-PIM2: 50 ± 8 %
DMSO: 34 ± 17 %
PIMi 5 µM: 44 ± 14 %
PIMi 10 µM: 50 ± 12 %
PIM 20 µM: 55 ± 16 %
PIMi 40 µM: 69 ± 18 %
K
L
PIMi :

Fig. 4

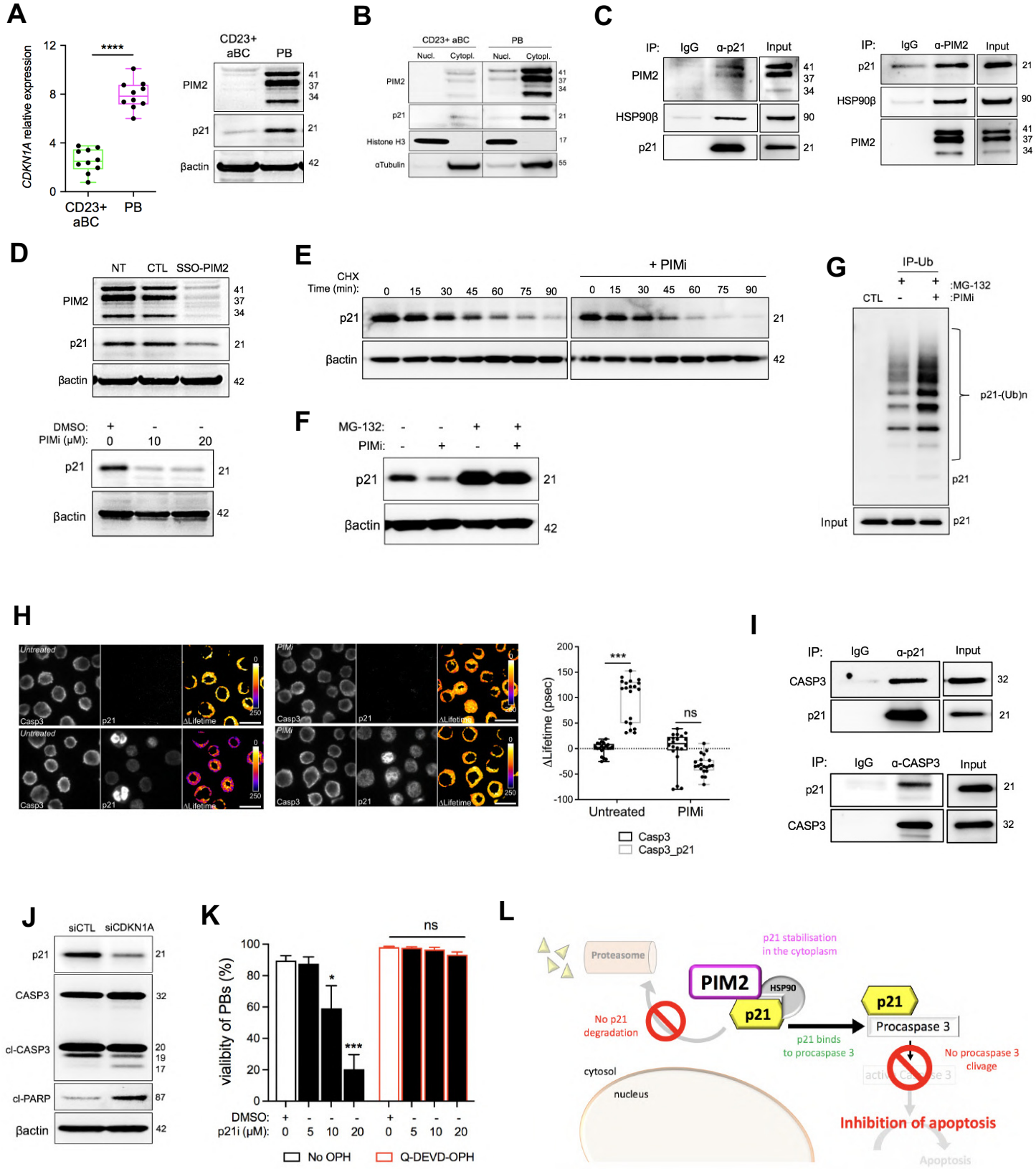

A
CDKN1A relative expression
****
CD23+ aBC
PB
PIM2
p21
βactin
B
Nucl.
Cytopl.
Histone H3
αTubulin
C
IP:
IgG
α-p21
Input
HSP90β
α-PIM2
D
NT
CTL
SSO-PIM2
DMSO:
PIMi (μM):
E
CHX
Time (min):
+ PIMi
F
MG-132:
PIMi:
G
IP-Ub
:MG-132
:PIMi
p21-(Ub)n
H
Untreated
PIMi
Casp3
ΔLifetime
ΔLifetime (psec)
Casp3_p21
I
CASP3
J
siCTL
siCDKN1A
cl-CASP3
cl-PARP
K
viability of PBs (%)
DMSO:
p21i (μM):
No OPH
Q-DEVD-OPH
L
Proteasome
p21 stabilisation in the cytoplasm
PIM2
HSP90
No p21 degradation
p21 binds to procaspase 3
Procaspase 3
No procaspase 3 clivage
cytosol
nucleus
Inhibition of apoptosis
Apoptosis

Fig. 5

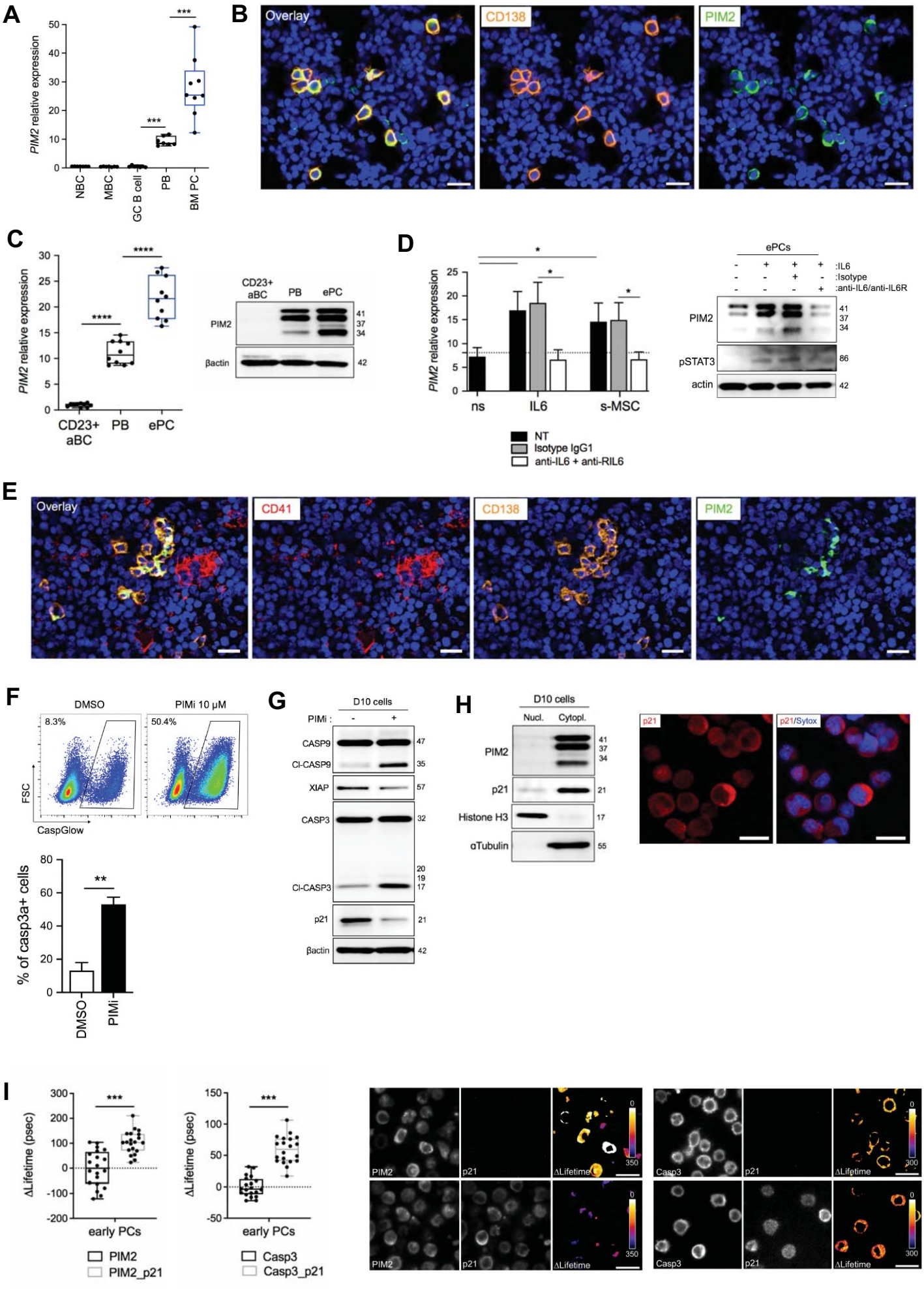

A
PIM2 relative expression
NBC
MBC
GC B cell
PB
BM PC
B
Overlay
CD138
PIM2
C
PIM2 relative expression
CD23+ aBC
PB
ePC
PIM2
βactin
D
PIM2 relative expression
ns
IL6
s-MSC
NT
Isotype IgG1
anti-IL6 + anti-RIL6
ePCs
:IL6
:Isotype
:anti-IL6/anti-IL6R
PIM2
pSTAT3
actin
E
Overlay
CD41
CD138
PIM2
F
DMSO
PIMi 10 µM
8.3%
50.4%
FSC
CaspGlow
% of casp3a+ cells
DMSO
PIMi
G
D10 cells
PIMi :
CASP9
Cl-CASP9
XIAP
CASP3
Cl-CASP3
p21
βactin
H
D10 cells
Nucl.
Cytopl.
PIM2
p21
Histone H3
αTubulin
p21
p21/Sytox
I
ΔLifetime (psec)
early PCs
PIM2
PIM2_p21
Casp3
Casp3_p21
PIM2
p21
ΔLifetime
Casp3

Fig. 6

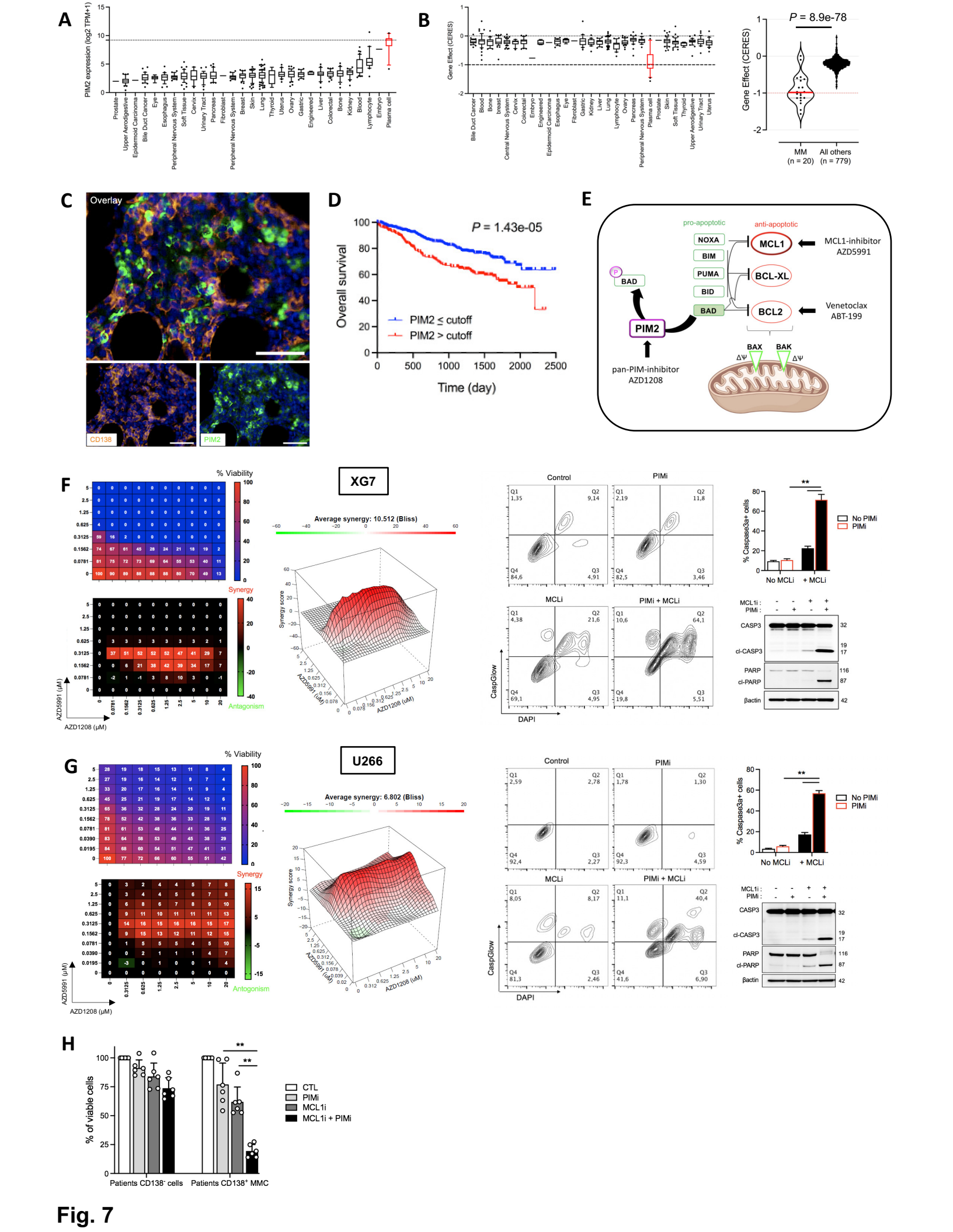

A
PIM2 expression (log2 TPM+1)
Prostate
Upper Aerodigestive
Epidermoid Carcinoma
Bile Duct Cancer
Eye
Esophagus
Peripheral Nervous System
Soft Tissue
Cervix
Urinary Tract
Pancreas
Fibroblast
Peripheral Nervous System
Breast
Skin
Lung
Thyroid
Uterus
Ovary
Gastric
Engineered
Liver
Colorectal
Bone
Kidney
Blood
Lymphocyte
Embryo
Plasma cell
B
Gene Effect (CERES)
Bile Duct Cancer
Blood
Bone
Breast
Central Nervous System
Cervix
Colorectal
Embryo
Engineered
Epidermoid Carcinoma
Esophagus
Eye
Fibroblast
Gastric
Kidney
Liver
Lung
Lymphocyte
Ovary
Pancreas
Peripheral Nervous System
Plasma cell
Prostate
Skin
Soft Tissue
Thyroid
Upper Aerodigestive
Urinary Tract
Uterus
P = 8.9e-78
Gene Effect (CERES)
MM (n = 20)
All others (n = 779)
C
Overlay
CD138
PIM2
D
P = 1.43e-05
Overall survival
PIM2 ≤ cutoff
PIM2 > cutoff
Time (day)
E
pro-apoptotic
anti-apoptotic
NOXA
BIM
PUMA
BID
BAD
MCL1
BCL-XL
BCL2
MCL1-inhibitor
AZD5991
Venetoclax
ABT-199
P
BAD
PIM2
pan-PIM-inhibitor
AZD1208
BAX
BAK
ΔΨ
ΔΨ
F
% Viability
Synergy
Antagonism
AZD5991 (μM)
AZD1208 (μM)
XG7
Average synergy: 10.512 (Bliss)
Synergy score
Control
PIMi
MCLi
PIMi + MCLi
CaspGlow
DAPI
% Caspase3a+ cells
No PIMi
PIMi
No MCLi
+ MCLi
MCL1i :
PIMi :
CASP3
cl-CASP3
PARP
cl-PARP
βactin
G
% Viability
Synergy
Antogonism
AZD5991 (μM)
AZD1208 (μM)
U266
Average synergy: 6.802 (Bliss)
Synergy score
Control
PIMi
MCLi
PIMi + MCLi
CaspGlow
DAPI
% Caspase3a+ cells
No PIMi
PIMi
No MCLi
+ MCLi
MCL1i :
PIMi :
CASP3
cl-CASP3
PARP
cl-PARP
βactin
H
% of viable cells
CTL
PIMi
MCL1i
MCL1i + PIMi
Patients CD138- cells
Patients CD138+ MMC

Fig. 7